

On the Convergence of Deep Learning with Differential Privacy

Zhiqi Bu* Hua Wang Qi Long Weijie J. Su

University of Pennsylvania
 {zbu, wanghua, qlong, suw}@upenn.edu

Abstract

In deep learning with differential privacy (DP), the neural network achieves the privacy usually at the cost of slower convergence (and thus lower performance) than its non-private counterpart. This work gives the first convergence analysis of the DP deep learning, through the lens of training dynamics and the neural tangent kernel (NTK). Our convergence theory successfully characterizes the effects of two key components in the DP training: the per-sample clipping (flat or layerwise) and the noise addition. Our analysis not only initiates a general principled framework to understand the DP deep learning with any network architecture and loss function, but also motivates a new clipping method – the *global clipping*, that significantly improves the convergence while preserving the same privacy guarantee as the existing *local clipping*.

In terms of theoretical results, we establish the precise connection between the per-sample clipping and NTK matrix. We show that in the *gradient flow*, i.e., with infinitesimal learning rate, the noise level of DP optimizers does not affect the convergence. We prove that DP gradient descent (GD) with global clipping guarantees the monotone convergence to zero loss, which can be violated by the existing DP-GD with local clipping. Notably, our analysis framework easily extends to other optimizers, e.g., DP-Adam. Empirically speaking, DP optimizers equipped with global clipping perform strongly on a wide range of classification and regression tasks. In particular, our global clipping is surprisingly effective at learning *calibrated classifiers*, in contrast to the existing DP classifiers which are oftentimes over-confident and unreliable. Implementation-wise, the new clipping can be realized by adding one line of code into the `Opacus` library.

1 Introduction

Deep learning has achieved tremendous success in many applications that involve crowdsourced information, e.g., face image, emails, financial status, and medical records. However, using such sensitive data raises severe privacy concerns on a range of image recognition, natural language processing and other tasks [12, 57, 52, 20, 21]. For a concrete example, researches have recently demonstrated multiple successful privacy attacks on deep learning models, in which the attackers can re-identify a member in the dataset using the location or the purchase record, via the membership inference attack [58, 14]. In another example, the attackers can extract a person’s name, email address, phone number, and physical address from the billion-parameter GPT-2 [56] via the extraction attack [15]. Therefore, many studies have applied differential privacy (DP) and its variants [28, 27, 29, 48, 26, 24], a mathematically rigorous approach, to protect against leakage of private information [3, 47, 46, 34]. To achieve this gold standard of privacy guarantee, since the seminal work [3], DP optimizers are applied to train the neural networks while preserving the accuracy of prediction. To name a few, researchers have proposed DP-SGD [3, 8], DP-Adam [9], DP-SGLD [62, 43], DP-FTRL [39], and DP-FedAvg [46].

Algorithmically speaking, DP optimizers generally have two extra steps in comparison to non-DP standard optimizers: the per-sample clipping and the random noise addition, so that DP optimizers descend in the direction of the averaged, clipped, noisy gradient (see Figure 1). These extra steps protect the resulting models against privacy attacks via the Gaussian mechanism [29, Theorem A.1], at the expense of an empirical performance degradation compared to the non-DP deep learning, in terms of much slower convergence and lower utility. For example, state-of-the-art CIFAR10 accuracy with DP is $\approx 60\%$ without pre-training [53] (while non-DP networks can achieve 90% accuracy) and similar performance drops have been observed on facial images, tweets, and many other datasets [7].

*Github: https://github.com/woodyx218/opacus_global_clipping.

Empirically, much work has evaluated the effects of noise scale, batch size, clipping norm, learning rate, and network architecture on the privacy-accuracy trade-off [3, 53]. However, despite the prevalent usage of DP optimizers, little is known about the convergence behaviors from a theoretical viewpoint, which is necessary to understand and improve the deep learning with differential privacy. We notice one previous attempt by [17], analyzing the DP-SGD convergence through an assumption of symmetric gradient distribution, which can be unrealistic and inapplicable to real datasets.

Our Contributions In this work, we establish a principled framework to analyze the dynamics of DP deep learning, which helps demystify the phenomenon of the privacy-accuracy trade-off. Our contributions are four-fold:

- We explicitly characterize the *general training dynamics* of deep learning with DP gradient methods (e.g., DP-GD and DP-Adam). We show a fundamental influence of the DP training on the NTK matrix. This analysis leads to a *convergence theory* for the DP deep learning.
- On top of our convergence analysis, we propose a principle for designing the DP optimizers and thus develop a new *global clipping* method that provably enjoys desirable convergence behaviors.
- We demonstrate via numerous experiments that DP optimizers with global clipping significantly improve the loss convergence. Interestingly, this further effectively mitigates the *calibration* issue of existing DP classifiers, which are usually overly “confident”.
- Practically speaking, the global clipping is *easy-to-code* (see Appendix D) and *generalizable* to arbitrary optimizers, network architectures, and loss functions, with the *same privacy guarantee* and *computational efficiency* as the local clipping.

To elaborate on the study of *calibration* [36, 51], a critical performance measure besides accuracy and privacy, we give a concrete example: a binary classifier is calibrated if it predicts with 80% confidence (the probability assigned on its output class) and has an average accuracy close to 80%, i.e., this classifier’s confidence matches its ability. We observe that DP models using the local clipping are oftentimes over-confident and hence unreliable, while the global clipping is amazingly effective on mitigating the mis-calibration. A quick preview of the comparison among the DP optimizers with the local and the global clipping is as follows:

Clipping type	Positive NTK	Loss convergence	Monotone loss decay	Zero loss
No clipping	Yes	Yes	Yes	Yes
Local & Flat	No	No	No	Yes
Local & Layer	No	No	No	No
Global & Flat	Yes	Yes	Yes	Yes
Global & Layer	Yes	Yes	Yes	Yes

Table 1: Effects of different per-sample clippings on deep learning with DP-GD. Here “Yes/No” means guaranteed or not. The loss refers to the training set. “Loss convergence” is conditioned on $\mathbf{H}(t) \succ 0$ (defined in (2.1)). “Zero loss” is measured at the terminal phase of training.

2 Warmup: Convergence of Non-Private Gradient Descent

We start by reviewing the standard, non-DP Gradient Descent (GD) for *arbitrary neural network* and *arbitrary loss*, before we dive into the analysis of DP optimizers. In particular, we analyze the training dynamics of a neural network using the neural tangent kernel (NTK) matrix¹.

Suppose we have a neural network f governed by weights \mathbf{w} , with samples \mathbf{x}_i and labels y_i ($i = 1, \dots, n$). Denote the prediction by $f_i = f(\mathbf{x}_i)$, and the per-sample loss by $\ell_i = \ell(f(\mathbf{x}_i, \mathbf{w}), y_i)$ for some loss function ℓ .

¹We emphasize that our analysis works on any neural networks, not limited to the infinitely wide or over-parameterized ones. Put differently, we don’t assume the NTK matrix \mathbf{H} to be deterministic nor nearly time-independent, as was the case in [5, 42, 25, 4, 64, 31, 6].

We define the objective function L to be the average of per-sample losses

$$L(\mathbf{w}) = \frac{1}{n} \sum_{i=1}^n \ell(f(\mathbf{x}_i, \mathbf{w}), y_i).$$

The discrete gradient descent, with a step size η , can be written as:

$$\mathbf{w}(k+1) = \mathbf{w}(k) - \eta \frac{\partial L}{\partial \mathbf{w}}^\top.$$

The corresponding *gradient flow*, i.e., the ordinary differential equation (ODE) describing the weight updates with infinitely small step size $\eta \rightarrow 0$ in the continuous time, is then:

$$\dot{\mathbf{w}}(t) = -\frac{\partial L}{\partial \mathbf{w}}^\top = -\frac{1}{n} \sum_i \nabla_{\mathbf{w}} \ell_i(t).$$

Applying the chain rules to the gradient flow, we obtain the following general dynamics of the loss L ,

$$\dot{L} = \frac{\partial L}{\partial \mathbf{w}} \dot{\mathbf{w}} = -\frac{\partial L}{\partial \mathbf{w}} \frac{\partial L}{\partial \mathbf{w}}^\top = -\frac{1}{n^2} \frac{\partial L}{\partial \mathbf{f}} \frac{\partial \mathbf{f}}{\partial \mathbf{w}} \frac{\partial \mathbf{f}}{\partial \mathbf{w}}^\top \frac{\partial L}{\partial \mathbf{f}} = -\frac{1}{n^2} \frac{\partial L}{\partial \mathbf{f}} \mathbf{H}(t) \frac{\partial L}{\partial \mathbf{f}}^\top, \quad (2.1)$$

where $\frac{\partial L}{\partial \mathbf{f}} = (\frac{\partial \ell_1}{\partial f_1}, \dots, \frac{\partial \ell_n}{\partial f_n}) \in \mathbb{R}^{1 \times n}$, and the Gram matrix $\mathbf{H}(t) := \frac{\partial \mathbf{f}}{\partial \mathbf{w}} \frac{\partial \mathbf{f}}{\partial \mathbf{w}}^\top \in \mathbb{R}^{n \times n}$ is known as the NTK matrix, which is positive semi-definite and crucial to analyzing the convergence behavior.

To give a concrete example, let ℓ be the MSE loss $\ell_i(\mathbf{w}) = (f(\mathbf{x}_i, \mathbf{w}) - y_i)^2$ and $L_{\text{MSE}} = \frac{1}{n} \sum_i \ell_i(\mathbf{w}) = \frac{1}{n} \sum_i (f_i - y_i)^2$, then $\dot{L}_{\text{MSE}} = -4(\mathbf{f} - \mathbf{y})^\top \mathbf{H}(t)(\mathbf{f} - \mathbf{y})/n^2$. Furthermore, if $\mathbf{H}(t)$ is positive definite, the MSE loss $L_{\text{MSE}} \rightarrow 0$ exponentially fast [25, 4, 64], the cross-entropy loss $L_{\text{CE}} \rightarrow 0$ at rate $O(1/t)$ and any loss convex in the prediction $L = \sum_i \ell_i/n$ converges to 0 [4].

3 Differentially Private Gradient Methods

We now introduce the DP optimizers [2, 1] to train the DP neural networks. One popular optimizer is the DP-SGD [59, 16, 3, 9] in Algorithm 1 and more optimizers such as DP-Adam can be found in Appendix G. In contrast to the standard SGD, the DP-SGD has two unique steps: the per-sample clipping (to guarantee the sensitivity of per-sample gradients) and the random noise addition (to guarantee the privacy of models), both discussed in details via the Gaussian mechanism in Lemma 5.2.

Algorithm 1 DP-SGD (with local or global flat per-sample clipping)

Parameters: initial weights \mathbf{w}_0 , learning rate η_t , subsampling probability p , number of iterations T , noise scale σ , gradient norm bound R .

for $t = 0, \dots, T - 1$ **do**

 Take a batch $I_t \subseteq \{1, \dots, n\}$ from training set D with subsampling probability p

for $i \in I_t$ **do**

$v_t^{(i)} \leftarrow \nabla_{\mathbf{w}} \ell(f(\mathbf{x}_i, \mathbf{w}_t), y_i)$

 Option 1: $C_i = \min \{1, R/\|v_t^{(i)}\|_2\}$ ▷ Local clipping factor

 Option 2: $C_i \equiv c = \min \{1, R/\max_{j \in D} \|v_t^{(j)}\|_2\}$ ▷ Global clipping factor

$\bar{v}_t^{(i)} \leftarrow C_i \cdot v_t^{(i)}$ ▷ Clip the gradient

$\bar{V}_t \leftarrow \sum_{i \in I_t} \bar{v}_t^{(i)}$ ▷ Sum over batch

$\mathbf{w}_{t+1} \leftarrow \mathbf{w}_t - \frac{\eta_t}{|I_t|} (\bar{V}_t + \sigma R \cdot \mathcal{N}(0, I))$ ▷ Apply Gaussian mechanism and descend

Particularly, although the per-sample clipping is widely applied in DP deep learning, its effect remains a mystery. Empirical observations have found that optimizers with the per-sample clipping have much worse convergence and accuracy [3, 7]. But the current form of clipping is heuristic and lacks theoretical understanding, especially when the noise addition is present.

In what follows, we propose and analyze a new clipping, namely the global clipping (see Option 2 in Algorithm 1), where the clipping norm of the i -th sample gradient depends on all other sample gradients, rather

than just on the i -th one as in the existing local clipping. More precisely, the clipping involves computing a clipping factor $0 < C_i \leq 1$ for each sample gradient and no clipping takes place if $C_i = 1$. While the local clipping multiplies C_i to $\nabla_{\mathbf{w}}\ell_i$, the global clipping applies the minimum factor $\min_i C_i$ to all $\{\nabla_{\mathbf{w}}\ell_i\}$. In this sense, the global per-sample clipping is indeed a batch clipping (see Appendix G.5 for further comparison). At the high level, the idea of global clipping is to preserve the gradient direction while bounding the sensitivity, which further guarantees the positive semi-definiteness of the NTK matrix via Theorem 2.

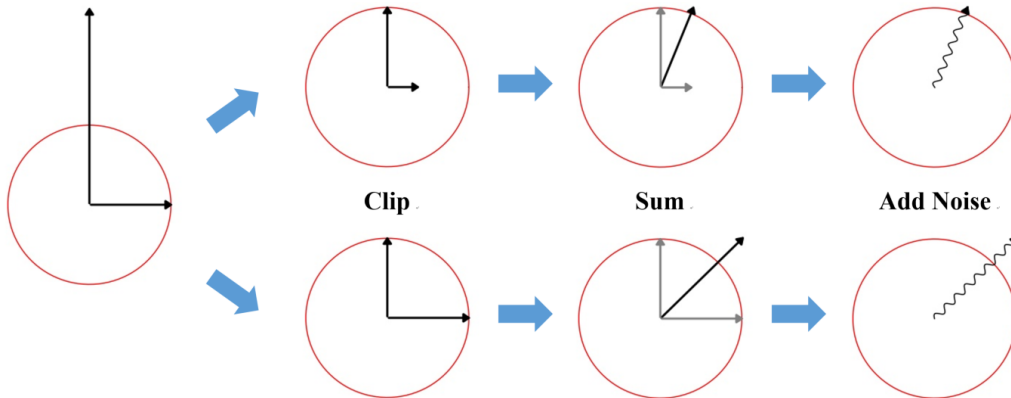


Figure 1: Illustration of global (upper) and local per-sample clipping (lower) in Algorithm 1. The black arrowed lines are two per-sample gradient vectors. The red circle has radius R .

4 DP Optimizers Convergence Analysis

In this section, we analyze the weight and loss dynamics of DP optimizers with the local or global per-sample clipping, denoted in the subscript, e.g., DP-SGD_{local} and DP-SGD_{global}. Our narrative here focuses on the most widely used DP-GD for the sake of simplicity, and our analysis generalizes to other full-batch DP optimizers such as DP-HeavyBall, DP-RMSprop, and DP-Adam as well, in Theorem 4 and Appendix G.

4.1 Effect of Noise Addition on Convergence

Our first result is easy yet surprising: the gradient flow of a stochastic noisy GD with non-zero noise (4.1) is the same as that of a deterministic dynamics without the noise (4.2). Put differently, the noise addition has no effect on the convergence of DP optimizers in the continuous time analysis. This is a common phenomenon called *certainty equivalence* in the stochastic control community [18].

To elaborate this point, we consider the DP-GD with Gaussian noise, as in Algorithm 1,

$$\mathbf{w}(k+1) = \mathbf{w}(k) - \frac{\eta}{n} \left(\sum_i \nabla_{\mathbf{w}}\ell_i C_i + \sigma R \cdot \mathcal{N}(0, 1) \right). \quad (4.1)$$

Notice that this general dynamics covers both the non-DP GD ($\sigma = 0$ and/or $C_i \equiv 1$) and DP-GD with local or global clipping ($C_i \equiv c$). Through Fact 4.1, we claim that the gradient flow of (4.1) is the same ODE regardless of the value of σ , and prove this in Appendix B.

Fact 4.1. For all $\sigma \geq 0$, the gradient descent in (4.1) corresponds to the continuous gradient flow

$$d\mathbf{w}(t) = -\frac{1}{n} \sum_i \nabla_{\mathbf{w}}\ell_i(t) C_i(t) dt. \quad (4.2)$$

This result indeed aligns the conventional wisdom² of tuning the clipping norm C first (e.g. setting $\sigma = 0.0$ or small) then the noise level σ , since the convergence is more sensitive to the clipping.

Remark 4.2. Our proof of Fact 4.1 shows that the certainty equivalence holds true generally for any DP optimizer besides DP-GD, i.e., different σ results in the same gradient flow as $\eta \rightarrow 0$.

²See https://github.com/pytorch/opacus/blob/master/tutorials/building_image_classifier.ipynb

4.2 Effect of Per-Sample Clipping on NTK Matrix

We move on to analyze the effect of the per-sample clipping on the DP training (4.2). It has been empirically observed that the per-sample clipping results in worse convergence and accuracy even without the noise [7]. We highlight that the NTK matrix is the key to understanding the convergence behavior and that the clipping affects NTK through its linear algebra properties, especially the positive semi-definiteness, which we define below in two notions for a *general* matrix.

Definition 4.3. For a (not necessarily symmetric) matrix A , it is

1. *positive in quadratic form* if and only if $\mathbf{x}^\top A \mathbf{x} > 0$ for every non-zero \mathbf{x} ;
2. *positive in eigenvalues* if and only if all eigenvalues of A are positive.

These two positivity definitions are equivalent for a symmetric or Hermitian matrix, but not for non-symmetric matrices. We illustrate this difference in Appendix A with some concrete examples. Next, we introduce two styles of per-sample clippings. Both can be implemented locally or globally.

Flat Clipping The DP-GD described in Algorithm 1 and (4.1), with the gradient flow (4.2), is equipped with the *flat* clipping [45]. In words, the flat clipping upper bounds the entire gradient vector by a norm R . Using the chain rules, we get

$$\dot{L} = \frac{\partial L}{\partial \mathbf{w}} \dot{\mathbf{w}} = -\frac{1}{n^2} \sum_j \nabla_{\mathbf{w}} \ell_j \sum_i \nabla_{\mathbf{w}} \ell_i C_i = -\frac{1}{n^2} \frac{\partial L}{\partial \mathbf{f}} \mathbf{H} \mathbf{C} \frac{\partial L}{\partial \mathbf{f}}^\top, \quad (4.3)$$

where $\mathbf{C}(t) = \text{diag}(C_1, \dots, C_n)$ is the clipping matrix at time t , with C_i defined in Algorithm 1. Note that for the global clipping, for all $i \in [n]$, we have the same $C_i \equiv c$, hence $\mathbf{C}(t) = c(t)\mathbf{I}$.

Layerwise Clipping. We additionally analyze another widely used clipping – the *layerwise* clipping [3, 46, 54]. Unlike the flat clipping, the layerwise clipping upper bounds the r -th layer’s gradient vector by a layer-dependent norm R_r , as demonstrated in Algorithm 2. Therefore, the DP-GD and its gradient flow with this layerwise clipping are:

$$\mathbf{w}_r(k+1) = \mathbf{w}_r(k) - \frac{\eta}{n} \left(\sum_i \nabla_{\mathbf{w}_r} \ell_i C_{i,r} + \sigma R_r \cdot \mathcal{N}(0, 1) \right) \quad \text{and} \quad \dot{\mathbf{w}}_r(t) = -\frac{1}{n} \sum_i \nabla_{\mathbf{w}_r} \ell_i C_{i,r}.$$

Then the loss dynamics is obtained by the chain rules:

$$\dot{L} = \sum_r \frac{\partial L}{\partial \mathbf{w}_r} \dot{\mathbf{w}}_r = -\frac{1}{n^2} \sum_r \frac{\partial L}{\partial \mathbf{f}} \mathbf{H}_r \mathbf{C}_r \frac{\partial L}{\partial \mathbf{f}}^\top, \quad (4.4)$$

where the layerwise NTK matrix $\mathbf{H}_r = \frac{\partial \mathbf{f}}{\partial \mathbf{w}_r} \frac{\partial \mathbf{f}}{\partial \mathbf{w}_r}^\top$, and $\mathbf{C}_r(t) = \text{diag}(C_{1,r}, \dots, C_{n,r})$.

In short, from (4.3) and (4.4), the per-sample clipping precisely changes the NTK matrix from \mathbf{H} , in standard non-DP deep learning, to $\mathbf{H} \mathbf{C}$ in DP training with flat clipping, and to $\sum_r \mathbf{H}_r \mathbf{C}_r$ in DP training with layerwise clipping. Subsequently, we will show two factors that worsen the convergence of DP training than the non-DP one:

- the local clipping may break NTK positivity and incur undesirable convergence behavior;
- the per-sample clipping reduces the eigenvalues of NTK and slows the convergence.

4.3 Local Per-Sample Clipping May Break NTK Positivity

We start with the analysis of local clipping, which is the prevailing clipping technique prior to our work. We show that the DP-GD with local clipping may break the positive semi-definiteness of the NTK matrix and cause non-monotone convergence³, which we empirically confirm in Figure 4.

³It is a fact that the product of a symmetric and positive definite matrices and a positive diagonal matrix may not be symmetric nor positive in quadratic form. This is shown in Appendix A.

Theorem 1. For an arbitrary neural network and a loss convex in f , suppose we clip the per-sample gradients **locally** in the gradient flow of DP-GD, and assume $\mathbf{H}(t) \succ 0$, then:

1. The local flat clipping has the loss dynamics in (4.3), with NTK matrix $\mathbf{H}(t)\mathbf{C}(t)$, which may not be symmetric nor positive in quadratic form, but is positive in eigenvalues.
2. The local layerwise clipping has the loss dynamics in (4.4), with NTK matrix $\sum_r \mathbf{H}_r(t)\mathbf{C}_r(t)$, which may not be symmetric nor positive in quadratic form or in eigenvalues.
3. For both local flat and layerwise clipping, the loss $L(t)$ may not decrease monotonically.
4. If the loss $L(t)$ converges, for the flat clipping, it converges to 0; for the layerwise clipping, it may converge to a non-zero value.

We prove Theorem 1 in Appendix B. The theorem states that breaking the positive definiteness of NTK by the local clipping may cause severe issues in the loss convergence, which is depicted in Figure 4. Therefore, we switch gears to analyzing the convergence of our global clipping.

4.4 Global Per-Sample Clipping Preserves NTK Positivity

Clearly the global clipping corresponds to symmetric and positive semi-definite NTK matrices $\mathbf{H}c$ in flat clipping and $\sum_r \mathbf{H}_r c_r$ in layerwise clipping, since all per-sample gradients share the same clipping factor. As a result, the clipping matrices are not only diagonal but indeed scalar in that $\mathbf{C} = c\mathbf{I}$ in (4.3) and $\mathbf{C}_r = c_r\mathbf{I}$ in (4.4). Hence we obtain the following result for the global clipping.

Theorem 2. For an arbitrary neural network and a loss convex in f , suppose we clip the per-sample gradients **globally** in the gradient flow of DP-GD, and assume $\mathbf{H}(t) \succ 0$, then:

1. The global flat (resp. layerwise) clipping has loss dynamics in (4.3) (resp. (4.4)), with NTK matrix $\mathbf{H}(t)c(t)$ (resp. $\sum_r \mathbf{H}_r(t)c_r(t)$); both NTK matrices are symmetric and positive definite.
2. For both global flat and layerwise clipping, the loss $L(t)$ decreases monotonically to 0.

We prove Theorem 2 in Appendix B and the benefits of the global clipping are assessed in Section 6. Our findings from Theorem 1 and Theorem 2 are visualized in the left plot of Figure 10 and summarized in Table 2, which further leads to Table 1.

Clipping method	NTK matrix	Symmetric matrix	Positive in quadratic form	Positive in eigenvalues
No clipping	\mathbf{H}	Yes	Yes	Yes
Local & Flat	$\mathbf{H}\mathbf{C}$	No	No	Yes
Local & Layerwise	$\sum_r \mathbf{H}_r \mathbf{C}_r$	No	No	No
Global & Flat	$\mathbf{H}c$	Yes	Yes	Yes
Global & Layerwise	$\sum_r \mathbf{H}_r c_r$	Yes	Yes	Yes

Table 2: Linear algebra properties of NTK by different clipping methods. Here ‘Yes/No’ means guaranteed or not.

4.5 Per-Sample Clipping Shrinks Spectrum of NTK Matrix

Here we briefly discuss the other factor that slows the DP training, i.e., that per-sample clipping reduces the eigenvalues of the NTK matrix. We leave the proof in Appendix B.

Proposition 4.4. Let $\lambda_j(A)$ denote the j -th largest eigenvalue of matrix A . We have $\lambda_j(\mathbf{H}\mathbf{C}) \leq \lambda_j(\mathbf{H})$ in flat clipping and $\lambda_j(\sum_r \mathbf{H}_r \mathbf{C}_r) \leq \lambda_j(\sum_r \mathbf{H}_r)$. The inequalities hold strictly if $C_i < 1$ for all $i \in [n]$ or if $C_{i,r} < 1$ for all $i \in [n]$ for at least some r .

As implied by Proposition 4.4, the decrease in eigenvalues potentially leads to the slow convergence, even in the case of the global clipping when the positivity of NTK is preserved: by (4.3), we have $-\frac{\partial L}{\partial \mathbf{f}} \mathbf{H} c \frac{\partial L}{\partial \mathbf{f}}^\top > -\frac{\partial L}{\partial \mathbf{f}} \mathbf{H} \frac{\partial L}{\partial \mathbf{f}}^\top$ if $c(t) < 1$. In words, the loss decreases at a slower rate whenever the global clipping is active.

5 DP Optimizers Privacy Analysis

In this section we define DP mathematically and prove that DP optimizers using the global clipping have the same privacy guarantee as those using the local clipping. Notice that for the privacy analysis, we work with the general DP optimizers, including those with mini-batches.

Definition 5.1. A randomized algorithm M is $(\epsilon, \delta)_D$ -differentially private (DP) if for any neighboring datasets S, S' differ by one sample in D , and for any event E ,

$$\mathbb{P}[M(S) \in E] \leq e^\epsilon \mathbb{P}[M(S') \in E] + \delta. \quad (5.1)$$

We highlight that this DP notion is slightly different and relaxed from the traditional DP where the neighboring datasets can differ in *any* sample, which is dataset-independent. We work with this constrained (ϵ, δ) -DP in order to guarantee that $c(t) = \min_i C_i(t)$ is not affected by adding or removing one training sample from S , which further assures that the sensitivity is indeed at most R after the clipping. We demonstrate the necessity of our notion and compare it to other similar DP notions in Appendix E.

Our dataset-dependent DP notion is similar to some existing notions in spirit, especially the per-instance DP [61] and the personalized DP [35, 44, 30, 38]. In fact, a traditionally DP algorithm is also DP under our relaxation, and the new DP generalizes the personalized-DP and the per-instance DP (see Table 4). As a consequence, our dataset-dependent DP only guarantees the privacy protection on training samples, while the traditional DP protects any sample. However, our DP may still provably protect some non-training samples as empirically observed in Figure 2, if a sample has a gradient norm that is no larger than the largest training gradient norm.

A common approach to guarantee DP when approximating a function g is via additive noise calibrated to g 's sensitivity [28]. This is known as the Gaussian mechanism and widely used in DP deep learning.

Lemma 5.2 (Theorem A.1 [29]; Theorem 2.7 [24]). *Define the ℓ_2 sensitivity of any function g to be $\Delta g = \sup_{S, S'} \|g(S) - g(S')\|_2$ where the supreme is over all neighboring (S, S') . Then the **Gaussian mechanism** $\hat{g}(S) = g(S) + \sigma \Delta g \cdot \mathcal{N}(0, \mathbf{I})$ is (ϵ, δ) -DP for some ϵ depending on (σ, n, p, δ) .*

In fact, it is not hard to see from Option 1&2 in Algorithm 1 that both global and local clipping have the same sensitivity (since the sensitivity is a maximum), which is upper bounded by R .

For the same differentially private mechanism, different privacy accountants (e.g., Moments accountant [3, 13], Gaussian differential privacy (GDP) [24, 9], Fourier accountant [41], each based on a different composition theory) accumulate the privacy risk $\epsilon(\sigma, n, p, \delta, T)$ differently over T iterations. The next result shows that DP optimizers with global clipping is as private as those with local clipping, independent of the choice of the privacy accountant.

Theorem 3. *DP optimizers with the local or global clipping are equally (ϵ, δ) -DP.*

Proof of Theorem 3. Under local and global clipping in Algorithm 1, each clipped gradient $\bar{v}_t^{(i)}$ has a norm bounded by R . Therefore, both clippings have the same sensitivity of $\bar{V}_t = \sum_{i \in I_t} \bar{v}_t^{(i)}$ and hence the same privacy risk, regardless which privacy accountant is adopted. \square

While a DP model by definition is resilient to all types of privacy attacks, we illustrate that DP-SGD_{global} offers similar privacy protection to DP-SGD_{local} against the membership inference attacks (MIA) in Figure 2. MIA is a common privacy attack by which the attacker aims to determine whether a given data point belongs to the sensitive training set [26, 38, 41, 48]. In our setting, the black-box attacker uses a logistic regression that only has access to the prediction logits and labels. The privacy vulnerability is characterized as the attack model's AUC. Needless to say, lower AUC is preferred.

6 Numerical Results

We highlight that the global clipping works with any DP optimizers (e.g., DP-Adam, DP-RMSprop, DP-FTRL[39], DP-SGD-JL[10], etc.) that employ the local clipping, with almost identical computational complexity (discussed in Appendix D). Empirically, DP optimizers with global clipping improve over existing DP optimizers

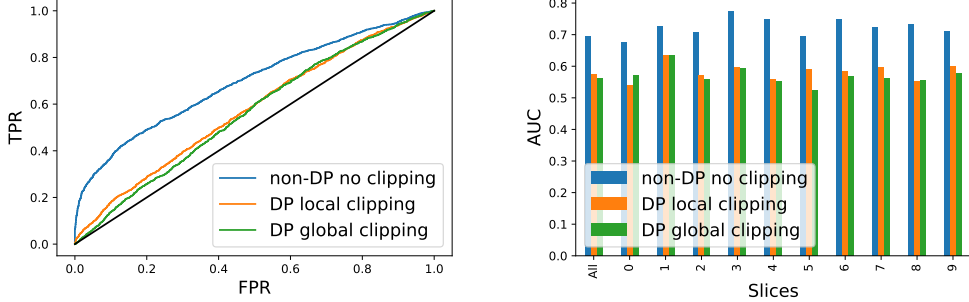


Figure 2: Attack model’s ROC-AUC on entire CIFAR10 in Section 6.1. Upper: non-DP overall AUC, 0.69; DP-SGD_{local}, 0.58; DP-SGD_{global}, 0.56. Lower: AUC on subsets of samples by label classes.

on the convergence of training and generalization losses. We thus reveal a novel phenomenon that DP optimizers play important roles in producing well-calibrated and reliable models.

In M -class classification problems, we denote the probability prediction for the i -th sample as $\boldsymbol{\pi}_i \in \mathbb{R}^M$ so that $f(\boldsymbol{x}_i) = \operatorname{argmax}(\boldsymbol{\pi}_i)$, then the accuracy is $\mathbf{1}\{f(\boldsymbol{x}_i) = y_i\}$. The confidence, i.e., the probability associated with the predicted class, is $\hat{P}_i := \max_{k=1}^M [\boldsymbol{\pi}_i]_k$ and a good calibration means the confidence is close to the accuracy⁴. Formally, we employ two popular calibration metrics from [49] and summarize in Table 3: the Expected Calibration Error (ECE), which is reflected by the distance between the solid and dashed lines of the same color in Figure 3,

$$\mathbb{E}_{\hat{P}_i} \left[\left| \mathbb{P}(f(\boldsymbol{x}_i) = y_i | \hat{P}_i = p) - p \right| \right],$$

and the Maximum Calibration Error (MCE)

$$\max_{p \in [0,1]} \left| \mathbb{P}(f(\boldsymbol{x}_i) = y_i | \hat{P}_i = p) - p \right|.$$

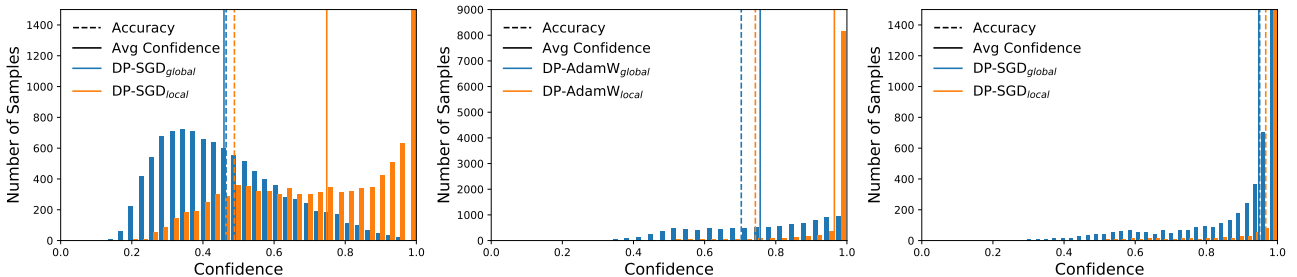


Figure 3: Confidence histograms on CIFAR 10 (left), SNLI (middle), and MNIST (right).

	ECE %			MCE %		
	non-DP	DP local	DP global	non-DP	DP local	DP global
CIFAR10	20.7	26.0	0.5	35.3	49.2	4.4
SNLI	13.0	22.2	5.3	34.7	62.5	12.5
MNIST	0.7	2.5	0.3	20.8	52.5	26.3

Table 3: Calibration metrics ECE and MCE by non-DP (no clipping) and DP optimizers.

Throughout this paper, we use the GDP privacy accountant for the experiments, with `Opacus` library under Apache License 2.0 and on a Google Colab P100 GPU. More details are available in Appendix F.

⁴An over-confident classifier, when predicting wrong at one data point, only reduces its accuracy a little but increases its loss significantly due to large $-\log(\pi_{y_i})$, since too little probability is assigned to the true class.

6.1 CIFAR10 image data with CNN model

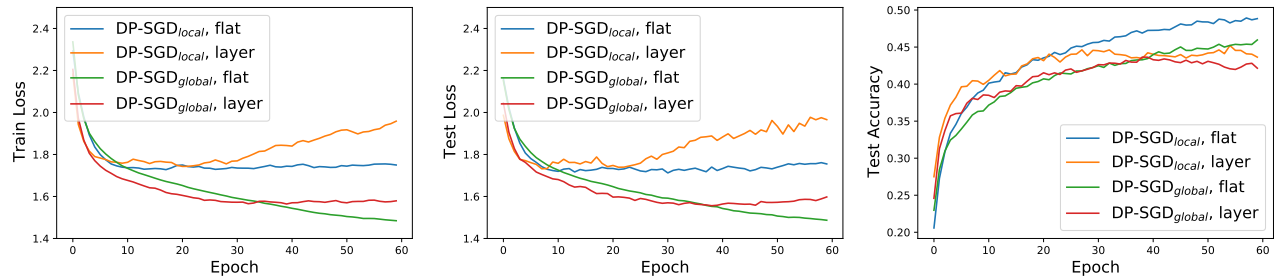


Figure 4: Loss (left and middle) and accuracy (right) on CIFAR10 with 4-layer CNN under different clipping methods, batch size 250, learning rate 0.05, noise scale 1.3, clipping norm 1.5 or $1.5 \cdot 1$.

We conduct experiments on the CIFAR10 dataset, which contains 50000 training samples and 10000 test samples of 32×32 color images in 10 classes. We use the standard CNN on Pytorch CIFAR10 tutorial⁵ (see Appendix F.2 for architecture) and train with DP-SGD without pre-training (unlike [3, 63], which pretrain on CIFAR100). Both clippings result in $(1.96, 10^{-5})$ -DP and the test accuracy (local: 48.84%; global: 45.96%) is comparable with state-of-the-art in [53], which is around 47%. Clearly from Figure 4, global clipping has better convergence and similar accuracy than local clipping. Especially, local layerwise clipping can be unstable, as indicated by Theorem 1. Notice that for classification tasks, the inconsistency between the optimization loss (cross-entropy) and the performance measure (accuracy) is not uncommon and even exaggerated in Section 6.2.

As indicated by the higher losses, the *confidence histogram* in Figure 3 shows the distribution of prediction confidence and validates that DP-SGD_{local} results in poorly calibrated classifiers (i.e., its 74.8% confidence is significantly higher than the 48.8% accuracy) but DP-SGD_{global} is well-calibrated, resulting in about 0.5% ECE.

In Figure 5, the *reliability diagram* [22, 51] displays the accuracy as a function of confidence. Graphically speaking, a calibrated classifier is expected to have blue bins close to the diagonal black dotted line. While the non-DP model is constantly over-confident and thus not calibrated, the global clipping effectively achieves nearly perfect calibration. In contrast, the classifier with local clipping is not only mis-calibrated, but also falls into ‘bipolar disorder’: it is either over-confident and inaccurate, or under-confident but highly accurate. This disorder is also observed in all other classification experiments in this paper. In addition, we also trained a large ResNet on CIFAR10 in Appendix F.3, with similar observations on the superior performance of global clipping.

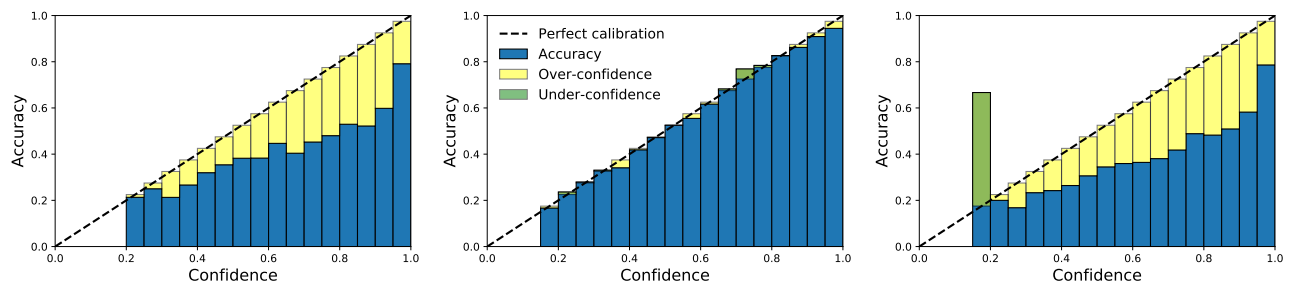


Figure 5: Reliability diagrams (left for non-DP; middle for global clipping; right for local clipping) on CIFAR10 with 4-layer CNN.

⁵See https://pytorch.org/tutorials/beginner/blitz/cifar10_tutorial.html.

6.2 SNLI text data with BERT model

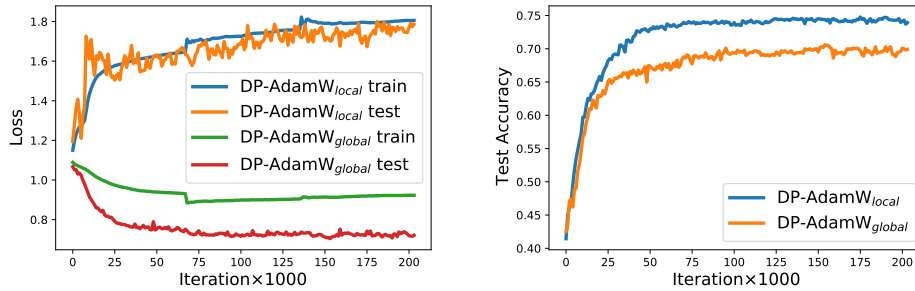


Figure 6: Loss (left) and accuracy (right) on SNLI with pre-trained BERT under different clipping methods, batch size 32, learning rate 0.0005, noise scale 0.4, clipping norm 0.1.

Stanford Natural Language Inference (SNLI)⁶ is a collection of human-written English sentence pairs with one of three classes: entailment, contradiction, or neutral. The dataset has 550152 training samples and 10000 test samples. We use the pre-trained BERT (Bidirectional Encoder Representations from Transformers) on `Opacus` tutorial⁷, which gives a state-of-the-art privacy-accuracy result. Our BERT contains 108M parameters and we only train the last Transformer encoder, which has 7M parameters, using DP-AdamW.

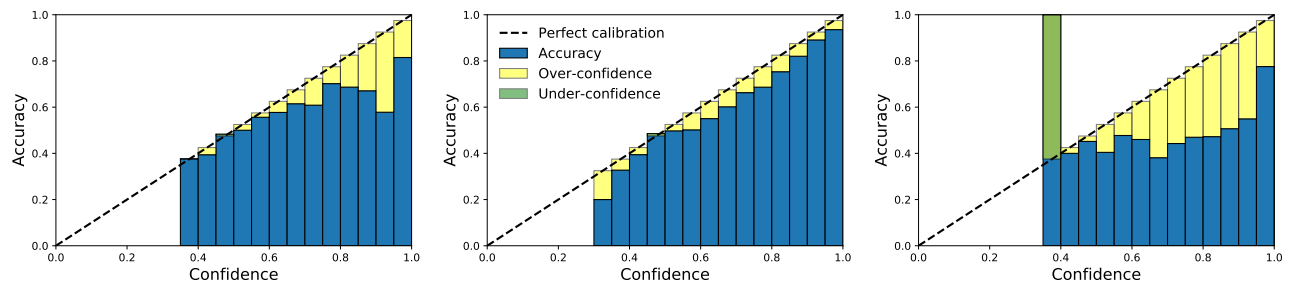


Figure 7: Reliability diagrams (left for non-DP; middle for global clipping; right for local clipping) on SNLI with BERT.

Surprisingly, the existing DP optimizer does not even minimize the loss at all, yet the accuracy still improves along the training. We again observe that global clipping has significantly better convergence, similar accuracy (local: 74.3%; global: 70.5%; non-DP: 85.4%), same privacy ($\epsilon = 1.25, \delta = 1/550152$), and much better calibration in comparison to the local clipping (see Table 3). The local clipping gives an ECE of about 22.2% and the global clipping about 5.3%. We remark that, to separate the effect of the global clipping from other factors like batch size, we keep the same hyperparameters as in the `Opacus` tutorial, which were tuned to be optimal for the local clipping. This is a disadvantage for the global clipping and the global clipping does not necessarily have worse accuracy, which we argue via the MNIST experiment.

6.3 MNIST image data with CNN model

On the MNIST dataset, which contains 60000 training samples and 10000 test samples of 28×28 grayscale images in 10 classes, we use the standard CNN in the DP libraries⁸[2, 1] (see Appendix F.1 for architecture) and train with DP-SGD. In Figure 8, both clippings result in $(2.32, 10^{-5})$ -DP, similar test accuracy (around 96.3%, the benchmark) and similar test loss. In contrast to Section 6.1 and Section 6.2, the MNIST experiment demonstrates that the global clipping does not necessarily need to trade off the accuracy for its advantage in the loss convergence and the calibration (see Figure 9).

⁶We use SNLI 1.0 from <https://nlp.stanford.edu/projects/snli/>

⁷See https://github.com/pytorch/opacus/blob/master/tutorials/building_text_classifier.ipynb.

⁸See <https://github.com/tensorflow/privacy/tree/master/tutorials> in Tensorflow and <https://github.com/pytorch/opacus/blob/master/examples/mnist.py> in Pytorch Opacus.

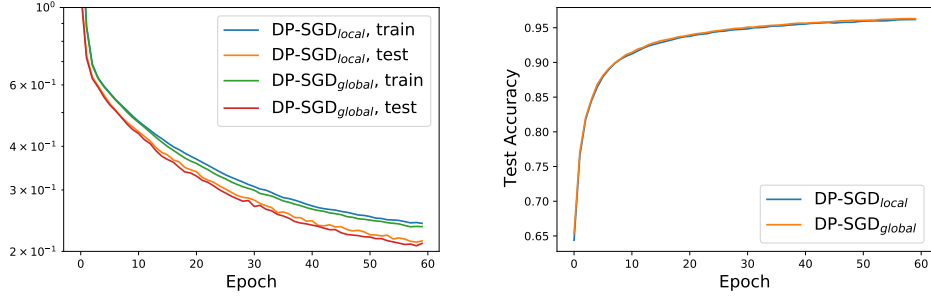


Figure 8: Loss (left) and accuracy (right) on MNIST with 3-layer CNN under different clipping methods, batch size 256, learning rate 0.15, noise scale 1.1, clipping norm 1.0.

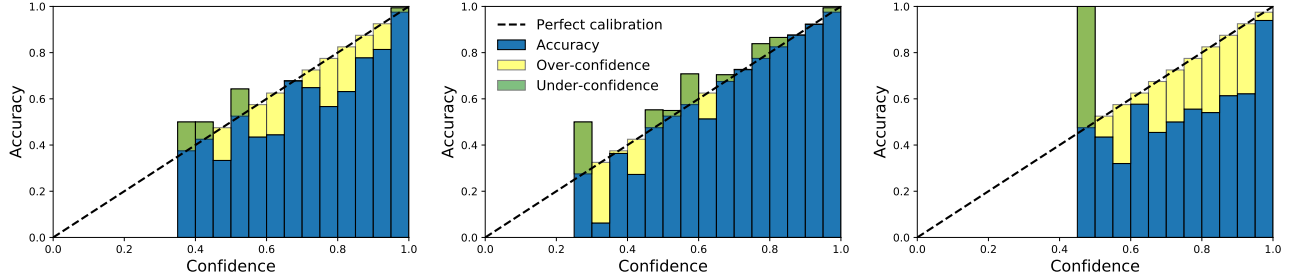


Figure 9: Reliability diagrams (left for non-DP; middle for global clipping; right for local clipping) on MNIST with 3-layer CNN. Batch size 256, learning rate 0.15, noise scale 1.1, clipping norm 1.0.

6.4 Regression Tasks

On regression tasks, the performance measure and the loss function are unified as MSE. Figure 10 shows that global clipping is comparable if not better than local clipping. We experiment on the California Housing data (20640 samples, 8 features) and Wine Quality (1599 samples, 11 features, run with full-batch DP-GD). Additional experiments trained with DP-GD are available in Appendix F.5.

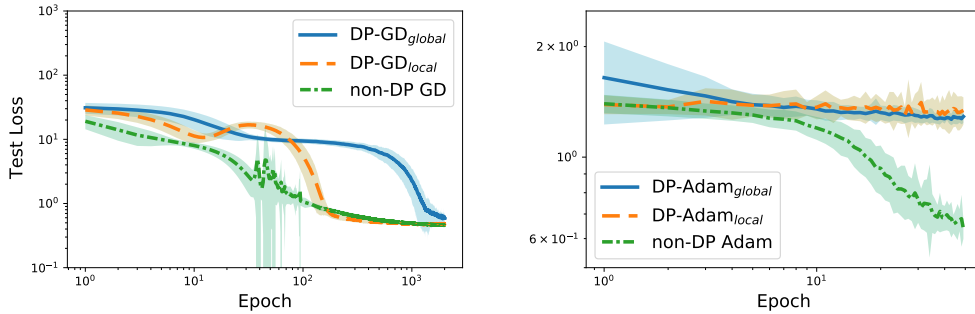


Figure 10: Performance of DP optimizers under different clipping methods on the Wine Quality (left) and the California Housing datasets (right). Experimental details in Appendix F.5.

7 Discussion

In this paper, we establish a framework of the convergence analysis for DP deep learning, via linear algebra properties of the NTK matrix. Our framework applies to general neural network architecture, loss function, and optimization algorithm. We show that in the continuous time analysis, the noise addition does not affect the convergence but the per-sample clipping does. We then propose the global clipping method, which has provable advantages in convergence with the same privacy guarantee as the existing local clipping. Our clipping can

outperform the local clipping in the sense of lower loss, better calibration, and comparable prediction accuracy.

A future direction is to study the discrete time convergence when the learning rate is not small. One immediate observation is that the noise addition will have an effect on the convergence, which needs further investigation. Another direction is to develop more fine-grained analysis, for instance, on the convergence rate of specific tasks, network architectures, or optimizers. This is an important problem because our current analysis focuses on the terminal phase of training, yet in practice, DP training usually stops before convergence due to the limited privacy budget. Lastly, the inconsistency between the cross-entropy loss and the prediction accuracy, as well as the connection to the calibration issue are intriguing; their theoretical understanding awaits future research.

Acknowledgement

We would like to thank Janardhan Kulkarni for stimulating discussions and encouragement. We also thank the **Opacus** team for maintaining this amazing library and for quick response to bugs. This work was supported in part by NSF through CCF-1763314, a Facebook Faculty Research Award, and NIH through R01GM124111 and RF1AG063481.

References

- [1] Pytorch Privacy library — Opacus.
<https://github.com/pytorch/opacus>.
- [2] Tensorflow Privacy library.
<https://github.com/tensorflow/privacy>.
- [3] M. Abadi, A. Chu, I. Goodfellow, H. B. McMahan, I. Mironov, K. Talwar, and L. Zhang. Deep learning with differential privacy. In *Proceedings of the 2016 ACM SIGSAC Conference on Computer and Communications Security*, pages 308–318, 2016.
- [4] Z. Allen-Zhu, Y. Li, and Z. Song. A convergence theory for deep learning via over-parameterization. In *International Conference on Machine Learning*, pages 242–252. PMLR, 2019.
- [5] S. Arora, S. S. Du, W. Hu, Z. Li, R. Salakhutdinov, and R. Wang. On exact computation with an infinitely wide neural net. *arXiv preprint arXiv:1904.11955*, 2019.
- [6] S. Arora, S. S. Du, W. Hu, Z. Li, and R. Wang. Fine-grained analysis of optimization and generalization for overparameterized two-layer neural networks. *arXiv preprint arXiv:1901.08584*, 2019.
- [7] E. Bagdasaryan, O. Poursaeed, and V. Shmatikov. Differential privacy has disparate impact on model accuracy. In *Advances in Neural Information Processing Systems*, pages 15453–15462, 2019.
- [8] R. Bassily, A. Smith, and A. Thakurta. Private empirical risk minimization: Efficient algorithms and tight error bounds. In *2014 IEEE 55th Annual Symposium on Foundations of Computer Science*, pages 464–473. IEEE, 2014.
- [9] Z. Bu, J. Dong, Q. Long, and W. J. Su. Deep learning with gaussian differential privacy. *arXiv preprint arXiv:1911.11607*, 2019.
- [10] Z. Bu, S. Gopi, J. Kulkarni, Y. T. Lee, J. H. Shen, and U. Tantipongpipat. Fast and memory efficient differentially private-sgd via jl projections. *arXiv preprint arXiv:2102.03013*, 2021.
- [11] Z. Bu, S. Xu, and K. Chen. A dynamical view on optimization algorithms of overparameterized neural networks. In *International Conference on Artificial Intelligence and Statistics*, pages 3187–3195. PMLR, 2021.
- [12] C. Cadwalladr and E. Graham-Harrison. Revealed: 50 million facebook profiles harvested for cambridge analytica in major data breach. *The guardian*, 17:22, 2018.

- [13] C. Canonne, G. Kamath, and T. Steinke. The discrete gaussian for differential privacy. *arXiv preprint arXiv:2004.00010*, 2020.
- [14] N. Carlini, C. Liu, Ú. Erlingsson, J. Kos, and D. Song. The secret sharer: Evaluating and testing unintended memorization in neural networks. In *28th {USENIX} Security Symposium ({USENIX} Security 19)*, pages 267–284, 2019.
- [15] N. Carlini, F. Tramer, E. Wallace, M. Jagielski, A. Herbert-Voss, K. Lee, A. Roberts, T. Brown, D. Song, U. Erlingsson, et al. Extracting training data from large language models. *arXiv preprint arXiv:2012.07805*, 2020.
- [16] K. Chaudhuri, C. Monteleoni, and A. D. Sarwate. Differentially private empirical risk minimization. *Journal of Machine Learning Research*, 12(3), 2011.
- [17] X. Chen, S. Z. Wu, and M. Hong. Understanding gradient clipping in private sgd: A geometric perspective. *Advances in Neural Information Processing Systems*, 33, 2020.
- [18] G. C. Chow et al. *Analysis and control of dynamic economic systems*. Wiley, 1975.
- [19] A. B. da Silva and M. Gazeau. A general system of differential equations to model first-order adaptive algorithms. *Journal of Machine Learning Research*, 21(129):1–42, 2020.
- [20] Y.-A. De Montjoye, C. A. Hidalgo, M. Verleysen, and V. D. Blondel. Unique in the crowd: The privacy bounds of human mobility. *Scientific reports*, 3(1):1–5, 2013.
- [21] Y.-A. De Montjoye, L. Radaelli, V. K. Singh, et al. Unique in the shopping mall: On the reidentifiability of credit card metadata. *Science*, 347(6221):536–539, 2015.
- [22] M. H. DeGroot and S. E. Fienberg. The comparison and evaluation of forecasters. *Journal of the Royal Statistical Society: Series D (The Statistician)*, 32(1-2):12–22, 1983.
- [23] N. Ding, Y. Fang, R. Babbush, C. Chen, R. Skeel, and H. Neven. Bayesian sampling using stochastic gradient thermostats. 2014.
- [24] J. Dong, A. Roth, and W. J. Su. Gaussian differential privacy. *arXiv preprint arXiv:1905.02383*, 2019.
- [25] S. S. Du, X. Zhai, B. Póczos, and A. Singh. Gradient descent provably optimizes over-parameterized neural networks. *arXiv preprint arXiv:1810.02054*, 2018.
- [26] J. C. Duchi, M. I. Jordan, and M. J. Wainwright. Local privacy and statistical minimax rates. In *2013 IEEE 54th Annual Symposium on Foundations of Computer Science*, pages 429–438. IEEE, 2013.
- [27] C. Dwork. Differential privacy: A survey of results. In *International conference on theory and applications of models of computation*, pages 1–19. Springer, 2008.
- [28] C. Dwork, F. McSherry, K. Nissim, and A. Smith. Calibrating noise to sensitivity in private data analysis. In *Theory of cryptography conference*, pages 265–284. Springer, 2006.
- [29] C. Dwork, A. Roth, et al. The algorithmic foundations of differential privacy. *Foundations and Trends in Theoretical Computer Science*, 9(3-4):211–407, 2014.
- [30] H. Ebadi, D. Sands, and G. Schneider. Differential privacy: Now it’s getting personal. *ACM Sigplan Notices*, 50(1):69–81, 2015.
- [31] S. Fort, G. K. Dziugaite, M. Paul, S. Kharaghani, D. M. Roy, and S. Ganguli. Deep learning versus kernel learning: an empirical study of loss landscape geometry and the time evolution of the neural tangent kernel. *arXiv preprint arXiv:2010.15110*, 2020.
- [32] W. Fulton. Eigenvalues, invariant factors, highest weights, and schubert calculus. *Bulletin of the American Mathematical Society*, 37(3):209–249, 2000.

- [33] I. M. Gel'fand and M. A. Naimark. The relation between the unitary representations of the complex unimodular group and its unitary subgroup. *Izvestiya Rossiiskoi Akademii Nauk. Seriya Matematicheskaya*, 14(3):239–260, 1950.
- [34] R. C. Geyer, T. Klein, and M. Nabi. Differentially private federated learning: A client level perspective. *arXiv preprint arXiv:1712.07557*, 2017.
- [35] A. Ghosh and A. Roth. Selling privacy at auction. In *Proceedings of the 12th ACM conference on Electronic commerce*, pages 199–208, 2011.
- [36] C. Guo, G. Pleiss, Y. Sun, and K. Q. Weinberger. On calibration of modern neural networks. In *International Conference on Machine Learning*, pages 1321–1330. PMLR, 2017.
- [37] K. He, X. Zhang, S. Ren, and J. Sun. Deep residual learning for image recognition. In *Proceedings of the IEEE conference on computer vision and pattern recognition*, pages 770–778, 2016.
- [38] Z. Jorgensen, T. Yu, and G. Cormode. Conservative or liberal? personalized differential privacy. In *2015 IEEE 31st international conference on data engineering*, pages 1023–1034. IEEE, 2015.
- [39] P. Kairouz, B. McMahan, S. Song, O. Thakkar, A. Thakurta, and Z. Xu. Practical and private (deep) learning without sampling or shuffling. *arXiv preprint arXiv:2103.00039*, 2021.
- [40] A. A. Klyachko. Random walks on symmetric spaces and inequalities for matrix spectra. *Linear Algebra and its Applications*, 319(1-3):37–59, 2000.
- [41] A. Koskela, J. Jälkö, and A. Honkela. Computing tight differential privacy guarantees using fft. In *International Conference on Artificial Intelligence and Statistics*, pages 2560–2569. PMLR, 2020.
- [42] J. Lee, L. Xiao, S. S. Schoenholz, Y. Bahri, R. Novak, J. Sohl-Dickstein, and J. Pennington. Wide neural networks of any depth evolve as linear models under gradient descent. *arXiv preprint arXiv:1902.06720*, 2019.
- [43] B. Li, C. Chen, H. Liu, and L. Carin. On connecting stochastic gradient mcmc and differential privacy. In *The 22nd International Conference on Artificial Intelligence and Statistics*, pages 557–566. PMLR, 2019.
- [44] Z. Liu, Y.-X. Wang, and A. Smola. Fast differentially private matrix factorization. In *Proceedings of the 9th ACM Conference on Recommender Systems*, pages 171–178, 2015.
- [45] H. B. McMahan, G. Andrew, U. Erlingsson, S. Chien, I. Mironov, N. Papernot, and P. Kairouz. A general approach to adding differential privacy to iterative training procedures. *arXiv preprint arXiv:1812.06210*, 2018.
- [46] H. B. McMahan, D. Ramage, K. Talwar, and L. Zhang. Learning differentially private recurrent language models. *arXiv preprint arXiv:1710.06963*, 2017.
- [47] F. McSherry and K. Talwar. Mechanism design via differential privacy. In *48th Annual IEEE Symposium on Foundations of Computer Science (FOCS'07)*, pages 94–103. IEEE, 2007.
- [48] I. Mironov. Rényi differential privacy. In *2017 IEEE 30th Computer Security Foundations Symposium (CSF)*, pages 263–275. IEEE, 2017.
- [49] M. P. Naeni, G. Cooper, and M. Hauskrecht. Obtaining well calibrated probabilities using bayesian binning. In *Proceedings of the AAAI Conference on Artificial Intelligence*, volume 29, 2015.
- [50] Y. E. Nesterov. A method for solving the convex programming problem with convergence rate $o(1/k^2)$. In *Dokl. akad. nauk Sssr*, volume 269, pages 543–547, 1983.
- [51] A. Niculescu-Mizil and R. Caruana. Predicting good probabilities with supervised learning. In *Proceedings of the 22nd international conference on Machine learning*, pages 625–632, 2005.
- [52] P. Ohm. Broken promises of privacy: Responding to the surprising failure of anonymization. *UCLA L. Rev.*, 57:1701, 2009.

- [53] N. Papernot, A. Thakurta, S. Song, S. Chien, and Ú. Erlingsson. Tempered sigmoid activations for deep learning with differential privacy. *arXiv preprint arXiv:2007.14191*, 2020.
- [54] N. Phan, X. Wu, H. Hu, and D. Dou. Adaptive laplace mechanism: Differential privacy preservation in deep learning. In *2017 IEEE International Conference on Data Mining (ICDM)*, pages 385–394. IEEE, 2017.
- [55] B. T. Polyak. Some methods of speeding up the convergence of iteration methods. *Ussr computational mathematics and mathematical physics*, 4(5):1–17, 1964.
- [56] A. Radford, J. Wu, R. Child, D. Luan, D. Amodei, and I. Sutskever. Language models are unsupervised multitask learners. *OpenAI blog*, 1(8):9, 2019.
- [57] L. Rocher, J. M. Hendrickx, and Y.-A. De Montjoye. Estimating the success of re-identifications in incomplete datasets using generative models. *Nature communications*, 10(1):1–9, 2019.
- [58] R. Shokri, M. Stronati, C. Song, and V. Shmatikov. Membership inference attacks against machine learning models. In *2017 IEEE Symposium on Security and Privacy (SP)*, pages 3–18. IEEE, 2017.
- [59] S. Song, K. Chaudhuri, and A. D. Sarwate. Stochastic gradient descent with differentially private updates. In *2013 IEEE Global Conference on Signal and Information Processing*, pages 245–248. IEEE, 2013.
- [60] J. Soria-Comas, J. Domingo-Ferrer, D. Sánchez, and D. Megías. Individual differential privacy: A utility-preserving formulation of differential privacy guarantees. *IEEE Transactions on Information Forensics and Security*, 12(6):1418–1429, 2017.
- [61] Y.-X. Wang. Per-instance differential privacy. *Journal of Privacy and Confidentiality*, 9(1), 2019.
- [62] Y.-X. Wang, S. Fienberg, and A. Smola. Privacy for free: Posterior sampling and stochastic gradient monte carlo. In *International Conference on Machine Learning*, pages 2493–2502. PMLR, 2015.
- [63] Z. Xu, S. Shi, A. X. Liu, J. Zhao, and L. Chen. An adaptive and fast convergent approach to differentially private deep learning. In *IEEE INFOCOM 2020-IEEE Conference on Computer Communications*, pages 1867–1876. IEEE, 2020.
- [64] D. Zou, Y. Cao, D. Zhou, and Q. Gu. Gradient descent optimizes over-parameterized deep relu networks. *Machine Learning*, 109(3):467–492, 2020.

A Linear Algebra Facts

Fact A.1. The product $A = M_1 M_2$, where M_1 is a symmetric and positive matrix and M_2 a positive diagonal matrix, is positive definite in eigenvalues but is non-symmetric in general (unless the diagonal matrix is constant) and non-positive in quadratic forms.

Proof of Fact A.1. To see the non-symmetry of A , suppose there exists i, j such that $(M_2)_{jj} \neq (M_2)_{ii}$, then

$$(M_1 M_2)_{ij} = \sum_k (M_1)_{ik} (M_2)_{kj} = (M_1)_{ij} (M_2)_{jj} = (M_1)_{ji} (M_2)_{jj},$$

$$(M_1 M_2)_{ji} = (M_1)_{ji} (M_2)_{ii} \neq (M_1)_{ji} (M_2)_{jj}.$$

Hence A is not symmetric and positive definite. To see that A may be non-positive in the quadratic form, we give a counter-example.

$$M_1 = \begin{pmatrix} 1 & 1 \\ 1 & 2 \end{pmatrix}, M_2 = \begin{pmatrix} 1 & 0 \\ 0 & 0.1 \end{pmatrix}, A = M_1 M_2 = \begin{pmatrix} 1 & 0.1 \\ 1 & 0.2 \end{pmatrix}, (1, -2)A \begin{pmatrix} 1 \\ -2 \end{pmatrix} = -0.4.$$

To see that A is positive in eigenvalues, we claim that an invertible square root $M_1^{1/2}$ exists as M_1 is symmetric and positive definite. Now A is similar to $(M_1^{1/2})^{-1} A M_1^{1/2} = M_1^{1/2} M_2 M_1^{1/2}$, hence the non-symmetric A has the same eigenvalues as the symmetric and positive definite $M_1^{1/2} M_2 M_1^{1/2}$. \square

Fact A.2. Matrix with all eigenvalues positive may be non-positive in quadratic form.

Proof of Fact A.2.

$$A = \begin{pmatrix} -1 & 3 \\ -3 & 8 \end{pmatrix}, (1, 0)A \begin{pmatrix} 1 \\ 0 \end{pmatrix} = -1,$$

though eigenvalues of A are $\frac{1}{2}(7 \pm 3\sqrt{5}) > 0$. \square

Fact A.3. Matrix with positive quadratic forms may have non-positive eigenvalues.

Proof of Fact A.3.

$$A = \begin{pmatrix} 1 & 1 \\ -1 & 1 \end{pmatrix}, (x, y)A \begin{pmatrix} x \\ y \end{pmatrix} = x^2 + y^2 > 0,$$

but eigenvalues of A are $1 \pm i$, not positive nor real. Actually, all eigenvalues of A always have positive real part. \square

Fact A.4. Sum of products of positive definite (symmetric) matrix and positive diagonal matrix may have zero or negative eigenvalues.

Proof of Fact A.4.

$$\mathbf{H}_1 = \begin{pmatrix} 8/9 & 2 \\ 2 & 7 \end{pmatrix}, \mathbf{C}_1 = \begin{pmatrix} 0.9 & 0 \\ 0 & 0.4 \end{pmatrix}, \mathbf{H}_2 = \begin{pmatrix} 3 & 2 \\ 2 & 2 \end{pmatrix}, \mathbf{C}_2 = \begin{pmatrix} 0.1 & 0 \\ 0 & 0.6 \end{pmatrix}.$$

Although \mathbf{H}_j are positive definite, $\mathbf{H}_1 \mathbf{C}_1 + \mathbf{H}_2 \mathbf{C}_2$ has a zero eigenvalue. Further, if $\mathbf{H}_1[1, 1] = 0.7$, $\mathbf{H}_1 \mathbf{C}_1 + \mathbf{H}_2 \mathbf{C}_2$ has a negative eigenvalue. \square

B Proof of Main Results

Proof of Fact 4.1. Expanding the discrete dynamic in (4.1) as $\mathbf{w}(k+1) = \mathbf{w}(k) - \frac{\eta}{n} \sum_i \nabla_{\mathbf{w}} \ell_i C_i - \frac{\eta \sigma R}{n} \mathcal{N}(0, 1)$, and chaining it for $r \geq 1$ times, we obtain

$$\mathbf{w}(k+r) - \mathbf{w}(k) = - \sum_{j=0}^{r-1} \frac{\eta}{n} \sum_i \nabla_{\mathbf{w}} \ell_i(\mathbf{w}(k+j)) C_i - \sum_{j=0}^{r-1} \frac{\eta \sigma R}{n} \mathcal{N}(0, 1).$$

In the limit of $\eta \rightarrow 0$, we re-index the weights \mathbf{w} by time, with $t = k\eta$ and $s = r\eta$. Then the left hand side becomes $\mathbf{w}(t+s) - \mathbf{w}(t)$; the first summation on the right hand side converges to $-\frac{1}{n} \int_t^{t+s} \sum_i \nabla_{\mathbf{w}} \ell_i(\tau) C_i(\tau) d\tau$, as long as the integral exists, and the second summation $J(\eta) = \sum_{j=0}^{r-1} \frac{\eta \sigma R}{n} \mathcal{N}(0, 1)$ has

$$\mathbb{E}[J(\eta)] = 0 \quad \text{and} \quad \text{Var}(J(\eta)) = \frac{\sigma^2 R^2 \eta^2}{n^2} r = \eta s \frac{\sigma^2 R^2}{n^2} \rightarrow 0, \text{ as } \eta \rightarrow 0.$$

Therefore, as $\eta \rightarrow 0$, the discrete stochastic dynamic (4.1) converges to a deterministic gradient flow given by the integral

$$\mathbf{w}(t) - \mathbf{w}(0) = -\frac{1}{n} \int_0^t \sum_i \nabla_{\mathbf{w}} \ell_i(\tau) C_i(\tau) d\tau,$$

which corresponds to the ordinary differential equations (4.2). \square

Proof of Theorem 1. We prove the statements using the derived gradient flow dynamics (4.2).

For Statement 1, from our narrative in Section 4.2 and Table 2, we know that the local flat clipping algorithm has $\mathbf{H}(t)\mathbf{C}(t)$ as its NTK. Since $\mathbf{H}(t)$ is positive definite and $\mathbf{C}(t)$ is a positive diagonal matrix, by Fact A.1, the product $\mathbf{H}(t)\mathbf{C}(t)$ is positive in eigenvalues, yet may be asymmetric and not positive in quadratic form in general.

Similarly, for Statement 2, we know the NTK of local layerwise clipping has the form $\sum_r \mathbf{H}_r(t)\mathbf{C}_r(t)$, which by Fact A.4 is asymmetric in general, and may be not positive in quadratic form nor positive in eigenvalues.

For Statement 3, by the training dynamics (4.3) for the local flat clipping algorithm and (4.4) for the local layerwise clipping, we see that \dot{L} equal the negation of a quadratic form of the corresponding NTK. By statement 1 & 2 of this theorem, such quadratic form may not be positive at all t , and hence the loss $L(t)$ is not guaranteed to decrease monotonically.

Lastly, for Statement 4, suppose $L(t)$ converges, i.e. $\dot{L} = 0 = \frac{\partial L}{\partial \mathbf{f}} \dot{\mathbf{f}}$. Suppose we have $L > 0$, then $\frac{\partial L}{\partial \mathbf{f}} \neq 0$ since L is convex in the prediction \mathbf{f} . In this case, we know $\dot{\mathbf{f}} = 0$. Observe that

$$0 = \dot{\mathbf{f}} = \frac{\partial \mathbf{f}}{\partial \mathbf{w}} \frac{\partial \mathbf{w}}{\partial t} = -\frac{\partial \mathbf{f}}{\partial \mathbf{w}} \frac{\partial \mathbf{f}}{\partial \mathbf{w}}^\top \frac{\partial L}{\partial \mathbf{f}}^\top.$$

For the local flat clipping, the NTK matrix, $\frac{\partial \mathbf{f}}{\partial \mathbf{w}} \frac{\partial \mathbf{f}}{\partial \mathbf{w}}^\top = \mathbf{H}\mathbf{C}$ is positive in eigenvalues (by Statement 1), so it could only be the case that $\frac{\partial L}{\partial \mathbf{f}} = \mathbf{0}$, contradicting to our premise that $L > 0$. Therefore we know $L = 0$ as long as it converges for the local flat clipping. On the other hand, for the local layerwise clipping, the NTK may be not positive in eigenvalues. Hence it is possible that $L \neq 0$ when $\dot{L} = 0$. \square

Proof of Theorem 2. The proof is similar to the previous proof, we consider the gradient flow dynamic for global clipping as follows:

For the first statement, we note that the NTKs for global clipping are obviously symmetric: since c and c_r are scalars, we have $(\mathbf{H}(t)c(t))^\top = \mathbf{H}(t)c(t)$, and $(\sum_r \mathbf{H}_r(t)c_r(t))^\top = \sum_r \mathbf{H}_r(t)c_r(t)$, are all symmetric matrices. Also, for all $x \neq 0$, $x^\top x \mathbf{H} x = c \cdot x^\top \mathbf{H} x > 0$, so the symmetric matrix $\mathbf{H}c$ is positive definite. Similar argument can easily show that the summation of symmetric positive matrices is also a positive definite matrix.

Now, to prove the second statement, we note that for both global flat clipping and global layerwise clipping, (4.3) and (4.4) give $\dot{L}(t) < 0$ since the NTKs are positive in quadratic form. That means L decreases monotonically. Additionally, L is bounded below by zero. Therefore L must converge and thus $\dot{L} = 0$. Note that when we have $\frac{\partial L}{\partial \mathbf{f}} = \mathbf{0}$, it implies all $\ell_i = 0$, and thus $L = 0$. \square

Lastly, we present the eigenvalues of NTK is indeed reduced after clipping.

Proof of Proposition 4.4 . Denoting the j -th largest singular value of matrix \mathbf{A} as $\sigma_j(\mathbf{A})$. Then for symmetric matrices H and C , we have $\sigma_j(\mathbf{H}) = \lambda_j(\mathbf{H})$, and $\sigma_j(\mathbf{C}) = \lambda_j(\mathbf{C}) \leq 1$. Via Weyl's theorem, we have $\lambda_j(\mathbf{H}\mathbf{C}) \leq \sigma_j(\mathbf{H}\mathbf{C})$. Furthermore, the following Horn's inequality is stated in [32, Theorem 16] and was proved in [33, 40],

$$\sigma_j(\mathbf{H}\mathbf{C}) \leq \sigma_j(\mathbf{H})\sigma_1(\mathbf{C}), \forall j. \tag{B.1}$$

So, we have

$$\lambda_j(\mathbf{HC}) \leq \sigma_j(\mathbf{HC}) \leq \sigma_j(\mathbf{H})\sigma_1(\mathbf{C}) = \lambda_j(\mathbf{H})\lambda_1(\mathbf{C}).$$

Since $\lambda_1(\mathbf{C}) \leq 1$, we know $\lambda_j(\mathbf{HC}) \leq \lambda_j(\mathbf{H})$. And further if the clipping is active for the batch (i.e. $C_i < 1$ for all i 's), then the eigenvalue of \mathbf{HC} is strictly less than that of \mathbf{H} . \square

C Layerwise Per-Sample Clipping

We elaborate the details of layerwise clipping in this section. We describe the layerwise clipping algorithm for DP-SGD, in complement to Algorithm 1 (not an generalization, i.e. flat clipping is not a subset of layerwise clipping). For other optimizers the extension to layerwise clipping is similar. Assume the neural network has d layers, denote the weights of the r -th layer as \mathbf{w}_r , then the layerwise clipping can clip the per-sample gradient of each layer either locally or globally.

Algorithm 2 DP-SGD (with local or global layerwise per-sample clipping)

Input: Dataset $S = \{(\mathbf{x}_1, y_1), \dots, (\mathbf{x}_n, y_n)\}$, loss function $\ell(f(\mathbf{x}_i, \mathbf{w}_t), y_i)$.

Parameters: initial weights \mathbf{w}_0 , learning rate η_t , subsampling probability p , number of iterations T , noise scale σ , gradient norm bound R_r for each layer $1 \leq r \leq d$.

for $t = 0, \dots, T - 1$ **do**

 Take a subsample $I_t \subseteq \{1, \dots, n\}$ from training set D with subsampling probability p

for $r = 1, \dots, d$ **do**

for $i \in I_t$ **do**

$v_{r,t}^{(i)} \leftarrow \nabla_{\mathbf{w}_r} \ell(f(\mathbf{x}_i, \mathbf{w}_t), y_i)$

 Option 1: $C_{i,r} = \min \{1, R_r / \|v_{r,t}^{(i)}\|_2\}$ ▷ Local clipping factor

 Option 2: $C_{i,r} \equiv c_r = \min \{1, R_r / \max_{j \in D} \|v_{r,t}^{(j)}\|_2\}$ ▷ Global clipping factor

$\bar{v}_{r,t}^{(i)} \leftarrow C_{i,r} \cdot v_{r,t}^{(i)}$ ▷ Clip the gradient

$\bar{V}_{r,t} \leftarrow \sum_{i \in I_t} \bar{v}_{r,t}^{(i)}$ ▷ Sum over batch

$\tilde{V}_{r,t} \leftarrow \bar{V}_{r,t} + \sigma R_r \cdot \mathcal{N}(0, I)$ ▷ Apply Gaussian mechanism

$\mathbf{w}_{r,t+1} \leftarrow \mathbf{w}_{r,t} - \frac{\eta_t}{|I_t|} \tilde{V}_{r,t}$ ▷ Descend

Output \mathbf{w}_T

For implementation, one can set `max_grad_norm` as a list of scalars in the `Opacus PrivacyEngine`⁹.

D Code Implementation

Building on top of the Pytorch `Opacus`¹⁰ library, we only need to add one line of code into `opacus/per_sample_gradient_clip.py`. This can be realized in multiple ways.

 Either we add

```
all_norms=[torch.max(each)+torch.zeros_like(each) for each in all_norms]
```

after line 181. Or we add

```
clipping_factor=[torch.min(each)+torch.zeros_like(each) for each in clipping_factor]
```

 after line 184. Or we add

```
clip_factor=torch.min(clip_factor)+torch.zeros_like(clip_factor)
```

after line 196 (within the for loop).

 Comparing to the original PyTorch implementation, our code only computes an additional maximum over B (batch size) values, the extra computational complexity is negligible.

⁹See https://github.com/pytorch/opacus/blob/e9983eced87619f683d84861c6503aca4e9287d1/opacus/privacy_engine.py

¹⁰see <https://github.com/pytorch/opacus> as for 2021/04/25.

E Differential Privacy Notions

In this section we extensively discuss our relaxation of (ϵ, δ) -DP in Definition 5.1. For the ease of illustration, we consider the ϵ -DP, i.e., $\delta = 0$, which is defined as

$$\epsilon = \sup_S \sup_{S': S \tilde{z} S'} \sup_E \log \frac{\mathbb{P}[M(S) \in E]}{\mathbb{P}[M(S') \in E]}.$$

Here $S \tilde{z} S'$ means explicitly that S and S' differ by a single data point z . We summarized some DP notions in Table 4 that includes some dataset-dependent notions.

	Data set	private target	parametrized by
ϵ -DP [28]	\sup_S	\sup_z	\mathcal{A} only
f-DP/GDP [24]	\sup_S	\sup_z	\mathcal{A} only
Rényi-DP [48]	\sup_S	\sup_z	\mathcal{A} only
Personalized-DP [35]	\sup_S	fixed z	\mathcal{A} and z
Individual-DP [60]	fixed S	\sup_z	\mathcal{A} and S
Per-instance DP [61]	fixed S	fixed z	\mathcal{A}, S and z
ϵ_D -DP (ours)	\sup_S	$\sup_{z \in D}$	\mathcal{A} and D

Table 4: Comparing variants of differential privacy.

We see that $\{M : M \text{ is } \epsilon\text{-DP}\} \subset \{M : M \text{ is } \epsilon_D\text{-DP}\}$ and furthermore $\{M : M \text{ is } \epsilon_D\text{-DP}\} \equiv \bigcup_{z \in D} \{M : M \text{ is } \epsilon\text{-personalized-DP}\} \equiv \bigcup_{S, z \in D} \{M : M \text{ is } \epsilon\text{-per-instance-DP}\}$.

We now give a simple example to demonstrate the necessity of such DP relaxation: consider 1-dimensional training set $D = \{1, 2, 3\}$ and clipping norm $R = 1$. Suppose we have two batches $S = \{1, 2\}, S' = \{1, 2, 3\}$, then $C_1 = 1, C_2 = 1/2, C_3 = 1/3$ and $c = \min C_i = 1/3$, regardless of the batch. As long as the differing sample belongs to D , even if say $S = \{1, 4, 5\}, S' = \{1, 3, 4, 5\}$, the difference between batches after clipping is at most R and hence applying $\sigma RN(0, 1)$ noise guarantees the DP (or indistinguishability) via the Gaussian mechanism.

F Experimental Details

F.1 MNIST

For MNIST, we use the standard CNN in `Tensorflow Privacy` and `Opacus`, as listed below. For both global and local clippings, the training hyperparameters (e.g. batch size) in Section 6.3 are exactly the same as reported in <https://github.com/tensorflow/privacy/tree/master/tutorials>, which gives 96.6% accuracy for the local clipping in Tensorflow and similar accuracy in Pytorch, where our experiments are conducted. The non-DP network is about 99% accurate. Notice the tutorial uses a different privacy accountant than the GDP that we used.

```
class SampleConvNet(nn.Module):
    def __init__(self):
        super().__init__()
        self.conv1 = nn.Conv2d(1, 16, 8, 2, padding=3)
        self.conv2 = nn.Conv2d(16, 32, 4, 2)
        self.fc1 = nn.Linear(32 * 4 * 4, 32)
        self.fc2 = nn.Linear(32, 10)

    def forward(self, x):
        # x of shape [B, 1, 28, 28]
        x = F.relu(self.conv1(x)) # -> [B, 16, 14, 14]
        x = F.max_pool2d(x, 2, 1) # -> [B, 16, 13, 13]
        x = F.relu(self.conv2(x)) # -> [B, 32, 5, 5]
        x = F.max_pool2d(x, 2, 1) # -> [B, 32, 4, 4]
```

```

x = x.view(-1, 32 * 4 * 4) # -> [B, 512]
x = F.relu(self.fc1(x)) # -> [B, 32]
x = self.fc2(x) # -> [B, 10]
return x

```

F.2 CIFAR10 with 4-layer CNN

In Section 6.1, we adopt the model from Pytorch tutorial in https://pytorch.org/tutorials/beginner/blitz/cifar10_tutorial.html, which is the following 4-layer CNN. The non-DP network is about 54% accurate.

```

class Net(nn.Module):
    def __init__(self):
        super().__init__()
        self.conv1 = nn.Conv2d(3, 6, 5)
        self.pool = nn.MaxPool2d(2, 2)
        self.conv2 = nn.Conv2d(6, 16, 5)
        self.fc1 = nn.Linear(16 * 5 * 5, 120)
        self.fc2 = nn.Linear(120, 84)
        self.fc3 = nn.Linear(84, 10)

    def forward(self, x):
        x = self.pool(F.relu(self.conv1(x)))
        x = self.pool(F.relu(self.conv2(x)))
        x = torch.flatten(x, 1) # flatten all dimensions except batch
        x = F.relu(self.fc1(x))
        x = F.relu(self.fc2(x))
        x = self.fc3(x)
        return x

```

In addition to Figure 3 and Figure 5, we plot in Figure 11 the distribution of prediction probability on the true class, say $[\pi_i]_{y_i}$ for the i -th sample (notice that Figure 3 plots $\max_k[\pi_i]_k$). Clearly the local clipping gives overly confident prediction: almost half of the time the true class is assigned close to zero prediction probability. The global clipping has a much more balanced prediction probability.

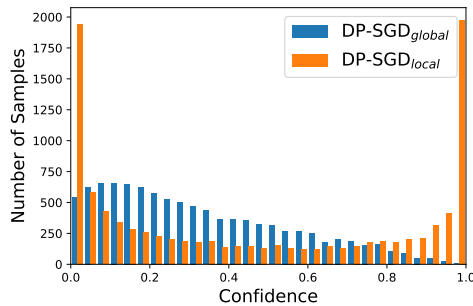


Figure 11: Prediction probability on the true class on CIFAR10 with 4-layer CNN.

F.3 CIFAR10 with ResNet

Following the Opacus tutorial in https://github.com/pytorch/opacus/blob/master/tutorials/building_image_classifier.ipynb, we further experiment a deep ResNet with 18 layers [37] on CIFAR10. Notice that BatchNorm violates DP so it is replaced by GroupNorm in the tutorial. The non-DP network is about 76% accurate. The local clipping gives 59.69% test accuracy and the global clipping gives 54.87% at $\epsilon = 53.54$ by

Pytorch’s Moments Accountant. Similar to Figure 4, we observe significant improvement in the loss convergence when using the global clipping.

We remark that our experiments use the same hyperparameters (batch size, noise scale, etc.) as in the Opacus tutorial, which were tuned to be optimal for the local clipping. It would be too quick to conclude that the global clipping has worse accuracy. The same statement applies to the SNLI experiment Section 6.2.

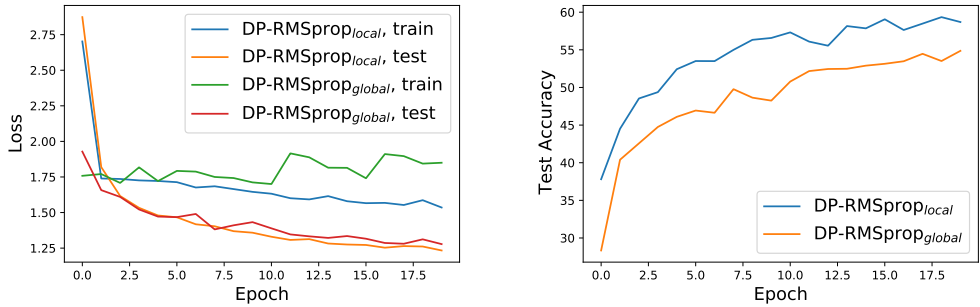


Figure 12: Loss (left) and accuracy (right) on CIFAR10 with 18-layer ResNet under different clipping methods, batch size 512, learning rate 0.001, noise 0.38, clipping norm 1.2.

F.4 NLP: SNLI with BERT model

In Section 6.2, we use the model from Opacus tutorial in https://github.com/pytorch/opacus/blob/master/tutorials/building_text_classifier.ipynb. The BERT architecture can be found in <https://github.com/pytorch/opacus/blob/master/tutorials/img/BERT.png>.

To train the BERT model, we do the standard pre-processing on the corpus (tokenize the input, cut or pad each sequence to MAX_LENGTH = 128, and convert tokens into unique IDs). We train the BERT model for 3 epochs. Similar to Appendix F.2, in addition to Figure 6 and Figure 7, we plot the distribution of prediction probability on the true class in Figure 13. Again, the local clipping is overly confident, with probability masses concentrating on the two extremes, yet the global clipping is more balanced in assigning the prediction probability.

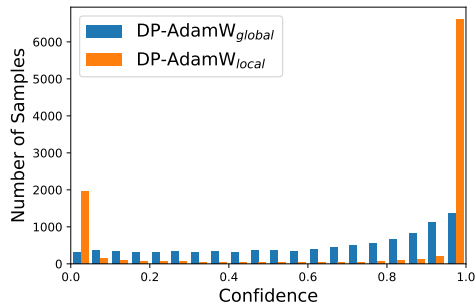


Figure 13: Prediction probability on the true class on SNLI with BERT.

F.5 Regression Experiments

In addition to the Wine Quality¹¹ (1279 training samples, 320 test samples, 11 features) and California Housing¹² (18576 training samples, 2064 test samples, 8 features) datasets in Section 6, we experiment on two more datasets: the Boston Housing¹³ (404 training samples, 102 test samples, 13 features) and Concrete Compressive

¹¹<http://archive.672ics.uci.edu/ml/datasets/Wine+Quality>
¹²<http://lib.stat.cmu.edu/datasets/houses.zip>
¹³<https://archive.ics.uci.edu/ml/machine-learning-databases/housing/>

Strength¹⁴ (824 training samples, 206 test samples, 8 features).

For the California Housing, we use DP-Adam with batch size 256. Since other datasets are not large, we use the full-batch DP-GD.

Across all the four experiments, we set $\delta = \frac{1}{1.1 \times \text{training sample size}}$ and use the four-layer neural network with the following structure, where `input_width` is the input dimension for each dataset:

```
class Net(nn.Module):
    def __init__(self, input_width):
        super(StandardNet, self).__init__()
        self.fc1 = nn.Linear(input_width, 64, bias = True)
        self.fc2 = nn.Linear(64, 64, bias = True)
        self.fc3 = nn.Linear(64, 32, bias = True)
        self.fc4 = nn.Linear(32, 1, bias = True)

    def forward(self, x):
        x = F.relu(self.fc1(x))
        x = F.relu(self.fc2(x))
        x = F.relu(self.fc3(x))
        return self.fc4(x)
```

The California Housing dataset is used to predict the mean price value of owner-occupied home in California. We train both global flat and local flat clipping with DP-Adam, both with noise $\sigma = 1$, clipping norm 1, and learning rate 0.0002. We also trained a non-DP GD with the same learning rate. The GDP accountant gives $\epsilon = 4.41$ after 50 epochs / 3650 iterations.

The UCI Wine Quality (red wine) dataset is used to predict the wine quality (an integer score between 0 and 10). We train both global flat and local flat clipping with DP-GD, both with noise $\sigma = 35$, clipping norm 2, and learning rate 0.03. We also trained a non-DP GD with learning rate 0.001. The GDP accountant gives $\epsilon = 4.40$ after 2000 iterations.

The California Housing and Wine Quality experiments are conducted in 30 independent runs. In Figure 10, the lines are the average losses and the shaded regions are the standard deviations.

The UCI Boston Housing dataset is used to predict the mean price value of owner-occupied home in Boston. We train both global flat and local flat clipping with DP-GD, both with noise $\sigma = 35$, clipping norm 1.1 and learning rate 0.015. The result is shown in the left plot of Figure 14. The GDP accountant gives $\epsilon = 2.83$ after 1197 iterations.

The Concrete Compressive Strength dataset is used to predict the concrete compressive strength. We train both global flat and local flat clipping using GD, both with noise $\sigma = 35$, clipping norm 1 and learning rate 0.03. The result is shown in the right plot of Figure 14. The GDP accountant gives $\epsilon = 2.90$ after 1097 iterations.

Similar to Figure 10, the global clipping achieves similar test MSE loss to the local clipping.

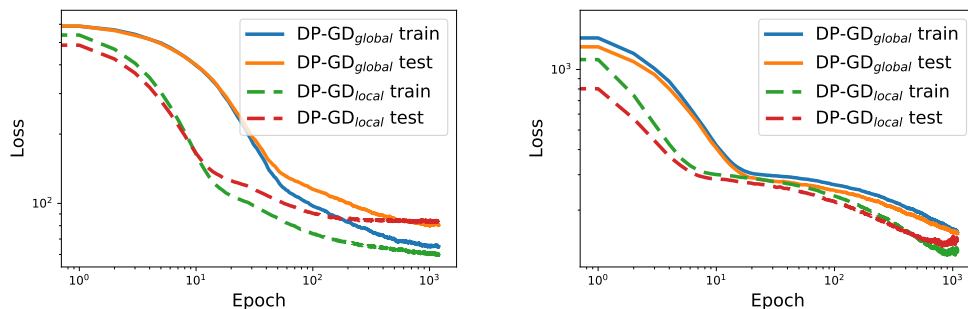


Figure 14: MSE loss on Boston Housing and Concrete Compressive Strength datasets under different clipping methods.

¹⁴<http://archive.ics.uci.edu/ml/datasets/Concrete+Compressive+Strength>

G Optimizers with Clipping beyond Gradient Descent

We can extend Theorem 1 and Theorem 2 to a wide class of full-batch optimizers besides DP-GD (with $\sigma = 0$ and $\sigma \neq 0$). We show that the NTK matrices in these optimizers determine whether the loss is zero if the model converges.

Theorem 4. *For an arbitrary neural network and a loss convex in f , suppose we clip the per-sample gradients in the gradient flow of Heavy Ball (HB), Nesterov Accelerated Gradient (NAG), Adam, ADAGRAD, RMSprop or their DP variants, and assume $\mathbf{H}(t) \succ 0$, then*

1. *if the loss $L(t)$ converges, it must converge to 0 for local flat, global flat and global layerwise clipping;*
2. *even if the loss $L(t)$ converges, it may converge to non-zero for local layerwise clipping.*

The proof can be easily extracted from that of Theorem 1 and Theorem 2 and hence is omitted. We highlight that DP optimizers in general correspond to deterministic gradient flow (for DP-GD, see Fact 4.1) – as long as the noise injected in each step is linear in step size. Therefore, the gradient flow is the same whether $\sigma > 0$ (the noisy case) or $\sigma = 0$ (the noiseless case).

We also note that the only difference between layerwise clipping and flat clipping is the form of NTK kernel, as we showed in Theorem 1 and Theorem 2. In this section, we will only present the result for flat clipping since its generalization to layerwise clipping is straightforward. In fact, part of the results for the global clipping has been implied by [11], which establishes the error dynamics for HB and NAG, but only on MSE loss and on specific network architecture. To analyze a broader class of optimizers and on the general loss and architecture, we turn to [19] which gives the dynamical systems of all optimizers aforementioned.

G.1 Gradient Methods with Momentum

We study two commonly used momentums, the Heavy Ball [55] and the Nesterov’s one [50]. These gradient methods correspond to the gradient flow system [19, Equation (2.1)]

$$\dot{\mathbf{w}}(t) = -\mathbf{m}(t), \tag{G.1}$$

$$\dot{\mathbf{m}}(t) = \sum_i \nabla_{\mathbf{w}} \ell_i C_i - r(t)\mathbf{m}(t). \tag{G.2}$$

We note that HB corresponds to time-independent $r(t) = r$ for some r and NAG corresponds to $r(t) = 3/t$. At the stationary point, we have $\dot{L} = \dot{\mathbf{w}} = \dot{\mathbf{m}} = 0$. Consequently (G.1) gives $\mathbf{m} = \mathbf{0}$ and (G.2) gives

$$\sum_i \nabla_{\mathbf{w}} \ell_i C_i = r\mathbf{m} = \mathbf{0}. \tag{G.3}$$

Multiplying both sides with $\frac{\partial \mathbf{f}}{\partial \mathbf{w}}$, we get

$$\mathbf{H}\mathbf{C} \frac{\partial L}{\partial \mathbf{f}} = \mathbf{0},$$

where $\frac{\partial L}{\partial \mathbf{f}}$ is defined in (4.3). If the NTK is positive in eigenvalues, as is the case for local flat and global clipping, we get $\frac{\partial L}{\partial \mathbf{f}} = \mathbf{0}$ and $\ell_i = 0$ for all i since the loss is convex (thus the only stationary point is the global minimum 0). Hence $L = 0$. Otherwise, e.g. for local layerwise clipping, it is possible that $\frac{\partial L}{\partial \mathbf{f}}^\top \neq \mathbf{0}$ and $L \neq 0$.

G.2 Adaptive Gradient Methods with Momentum

We consider Adam which corresponds to the dynamical system in [19, Equation (2.1)]

$$\dot{\mathbf{w}}(t) = -\mathbf{m}(t)/\sqrt{\mathbf{v}(t) + \xi}, \tag{G.4}$$

$$\dot{\mathbf{m}}(t) = \sum_i \nabla_{\mathbf{w}} \ell_i C_i - \frac{1}{\alpha_1} \mathbf{m}(t), \tag{G.5}$$

$$\dot{\mathbf{v}}(t) = \frac{1}{\alpha_2} \left[\sum_i \nabla_{\mathbf{w}} \ell_i C_i \right]^2 - \frac{1}{\alpha_2} \mathbf{v}(t). \tag{G.6}$$

Here $\xi \geq 0$ and the square is taken elementwise. At the stationary point, we have $\dot{L} = \dot{\mathbf{w}} = \dot{\mathbf{m}} = \dot{\mathbf{v}} = 0$. Consequently (G.4) gives $\mathbf{m} = \mathbf{0}$ and (G.5) gives $\sum_i \nabla_{\mathbf{w}} \ell_i C_i = \mathbf{m}/\alpha_1 = \mathbf{0}$. Multiplying both sides with $\frac{\partial f}{\partial \mathbf{w}}$, we get again $\mathbf{HC} \frac{\partial L}{\partial \mathbf{f}} = \mathbf{0}$, and hence the results follow.

G.3 Adaptive Gradient Methods without Momentum

We consider ADAGRAD and RMSprop which correspond to the dynamical system in [19, Remark 1]

$$\dot{\mathbf{w}}(t) = - \sum_i \nabla_{\mathbf{w}} \ell_i C_i / \sqrt{\mathbf{v}(t) + \xi}, \quad (\text{G.7})$$

$$\dot{\mathbf{v}}(t) = p(t) \left[\sum_i \nabla_{\mathbf{w}} \ell_i C_i \right]^2 - q(t) \mathbf{v}(t), \quad (\text{G.8})$$

for some $p(t), q(t)$. At the stationary point, we have $\dot{L} = \dot{\mathbf{w}} = \dot{\mathbf{m}} = \dot{\mathbf{v}} = 0$. Consequently (G.7) gives $\sum_i \nabla_{\mathbf{w}} \ell_i C_i = \mathbf{0}$. Multiplying both sides with $\frac{\partial f}{\partial \mathbf{w}}$, we get again $\mathbf{HC} \frac{\partial L}{\partial \mathbf{f}} = 0$, and hence the results follow.

G.4 Applying Global Clipping to DP Optimization Algorithms

Here we give some concrete algorithms where we can apply the global clipping method.

Many DP optimizers, non-adaptive (like HeavyBall and Nesterov Accelerated Gradient) and adaptive (like Adam, ADAGRAD), can use the global clipping easily. These optimizers are supported in `Opacus` and `Tensorflow Privacy` libraries. The original form of DP-Adam can be found in [9].

Algorithm 3 DP-Adam (with local or global per-sample clipping)

Input: Dataset $S = \{(\mathbf{x}_1, y_1), \dots, (\mathbf{x}_n, y_n)\}$, loss function $\ell(f(\mathbf{x}_i, \mathbf{w}_t), y_i)$.

Parameters: initial weights \mathbf{w}_0 , learning rate η_t , subsampling probability p , number of iterations T , noise scale σ , gradient norm bound R , momentum parameters (β_1, β_2) , initial momentum m_0 , initial past squared gradient u_0 , and a small constant $\xi > 0$.

for $t = 0, \dots, T - 1$ **do**

 Take a subsample $I_t \subseteq \{1, \dots, n\}$ from training set D with subsampling probability p

for $i \in I_t$ **do**

$v_t^{(i)} \leftarrow \nabla_{\mathbf{w}} \ell(f(\mathbf{x}_i, \mathbf{w}_t), y_i)$

 Option 1: $C_i = \min \{1, R / \|v_t^{(i)}\|_2\}$

 ▷ Local clipping factor

 Option 2: $C_i \equiv c = \min \{1, R / \max_{j \in D} \|v_t^{(j)}\|_2\}$

 ▷ Global clipping factor

$\bar{v}_t^{(i)} \leftarrow C_i \cdot v_t^{(i)}$

 ▷ Clip the gradient

$\tilde{v}_t \leftarrow \frac{1}{|I_t|} \left(\sum_{i \in I_t} \bar{v}_t^{(i)} + \sigma R \cdot \mathcal{N}(0, I) \right)$

 ▷ Apply Gaussian mechanism

$m_t \leftarrow \beta_1 m_{t-1} + (1 - \beta_1) \tilde{v}_t$

$u_t \leftarrow \beta_2 u_{t-1} + (1 - \beta_2) (\tilde{V}_t \odot \tilde{V}_t)$

 ▷ \odot is the Hadamard product

$\mathbf{w}_{t+1} \leftarrow m_t / (\sqrt{u_t} + \xi)$

 ▷ Descend

Output \mathbf{w}_T

Recently, [10] proposes to accelerate many DP optimizers with the JL projections in a memory efficient manner. Examples include DP-SGD-JL and DP-Adam-JL. The acceleration is achieved by only approximately instead of exactly computing the per-sample gradient norms. This does not affect the clipping operation afterwards and hence we can replace the local clipping currently used by our global clipping.

Algorithm 4 DP-SGD-JL (with local or global per-sample clipping)

Input: Dataset $S = \{(\mathbf{x}_1, y_1), \dots, (\mathbf{x}_n, y_n)\}$, loss function $\ell(f(\mathbf{x}_i, \mathbf{w}_t), y_i)$.

Parameters: initial weights \mathbf{w}_0 , learning rate η_t , subsampling probability p , number of iterations T , noise scale σ , gradient norm bound R , number of JL projections r .

for $t = 0, \dots, T - 1$ **do**

Take a subsample $I_t \subseteq \{1, \dots, n\}$ from training set D with subsampling probability p

Sample $u_1, \dots, u_r \sim \mathcal{N}(0, I)$

for $i \in I_t$ **do**

$v_t^{(i)} \leftarrow \nabla_{\mathbf{w}} \ell(f(\mathbf{x}_i, \mathbf{w}_t), y_i)$

for $j = 1$ to r **do**

$P_{ij} \leftarrow v_t^{(i)} \cdot u_j$ (using `dot`)

$M_i = \sqrt{\frac{1}{r} \sum_{j=1}^r P_{ij}^2}$

▷ M_i is an estimate for $\|v_t^{(i)}\|_2$.

Option 1: $C_i = \min\{1, R/M_i\}$

▷ Local clipping factor

Option 2: $C_i \equiv c = \min\{1, R/\max_{j \in D} M_j\}$

▷ Global clipping factor

$\bar{v}_t^{(i)} \leftarrow C_i \cdot v_t^{(i)}$

▷ Clip the gradient

$\bar{V} \leftarrow \sum_{i \in I_t} \bar{v}_t^{(i)}$

▷ Sum over batch

$\tilde{V}_t \leftarrow \bar{V}_t + \sigma R \cdot \mathcal{N}(0, I)$

▷ Apply Gaussian mechanism

$\mathbf{w}_{t+1} \leftarrow \mathbf{w}_t - \frac{\eta_t}{|I_t|} \tilde{V}_t$

▷ Descend

Output \mathbf{w}_T

In another line of research on the Bayesian neural networks, where the reliability of networks are emphasized, stochastic gradient Markov chain Monte Carlo (SG-MCMC) methods are applied to quantify the uncertainty of the weights. When DP is within the scope, one popular method is the DP stochastic gradient Langevin dynamics (DP-SGLD), where we can apply the global clipping.

Algorithm 5 DP-SGLD (with local or global per-sample clipping)

Input: Dataset $S = \{(\mathbf{x}_1, y_1), \dots, (\mathbf{x}_n, y_n)\}$, loss function $\ell(f(\mathbf{x}_i, \mathbf{w}_t), y_i)$.

Parameters: initial weights \mathbf{w}_0 , learning rate η_t , subsampling probability p , number of iterations T , gradient norm bound R , and a prior $p(\mathbf{w})$.

for $t = 0, \dots, T - 1$ **do**

Take a subsample $I_t \subseteq \{1, \dots, n\}$ from training set D with subsampling probability p

for $i \in I_t$ **do**

$v_t^{(i)} \leftarrow \nabla_{\mathbf{w}} \ell(f(\mathbf{x}_i, \mathbf{w}_t), y_i)$

Option 1: $C_i = \min\{1, R/\|v_t^{(i)}\|_2\}$

▷ Local clipping factor

Option 2: $C_i \equiv c = \min\{1, R/\max_{j \in D} \|v_t^{(j)}\|_2\}$

▷ Global clipping factor

$\bar{v}_t^{(i)} \leftarrow C_i \cdot v_t^{(i)}$

▷ Clip the gradient

$\bar{V} \leftarrow \sum_{i \in I_t} \bar{v}_t^{(i)}$

▷ Sum over batch

$\mathbf{w}_{t+1} \leftarrow \mathbf{w}_t - \eta_t \left(\frac{\bar{V}_t}{|I_t|} - \frac{\nabla_{\mathbf{w}} \log p(\mathbf{w})}{n} \right) + \mathcal{N}(0, \eta_t I)$

▷ Descend with Gaussian noise

Output \mathbf{w}_T

Here we treat \mathbf{w}_{t+1} as a posterior sample, instead of as a point estimate. Notice that other SG-MCMC methods such as SGNHT [23] can also be DP with the global per-sample clipping.

We emphasize that our global clipping applies whenever an optimization algorithm uses per-sample clipping. Therefore this appendix only gives a few example of the full capacity of global clipping.

G.5 Comparison between Different Clippings

Here we give a brief comparison between different clippings: the local per-sample clipping, the global per-sample clipping and the non-DP batch clipping (see Algorithm 6). In the example of SGD, the key difference between

Algorithm 6 Non-DP SGD (with batch clipping)

```
for  $t = 0, \dots, T - 1$  do
  Take a subsample  $I_t \subseteq \{1, \dots, n\}$  from training set  $D$  with subsampling probability  $p$ 
  for  $i \in I_t$  do
     $v_t^{(i)} \leftarrow \nabla_{\mathbf{w}} \ell(f(\mathbf{x}_i, \mathbf{w}_t), y_i)$ 
     $V_t \leftarrow \frac{1}{|I_t|} \sum_{i \in I_t} v_t^{(i)}$  ▷ Sum over batch
     $\bar{V}_t \leftarrow V_t \cdot \min\{1, R' / \|V_t\|_2\}$  ▷ Clip the gradient
     $\mathbf{w}_{t+1} \leftarrow \mathbf{w}_t - \eta_t \bar{V}_t$  ▷ Descend
Output  $\mathbf{w}_T$ 
```

the non-DP clipping and the DP clippings is the order of operations: the non-DP clipping first average the per-sample gradients, then clips in a batch manner. However, for DP clippings in Algorithm 1, we first clip the per-sample gradients (the local clipping works in a per-sample manner but the global clipping works in a batch manner) then take the average of the clipped gradients. Informally, we distinguish the gradients after different clippings as follows:

- **non-DP batch clipping:** $\bar{V}_t = \text{ave}(v_t^{(i)}) \cdot c' = \text{ave}(v_t^{(i)} \cdot c')$;
- **DP local per-sample clipping:** $\bar{V}_t = \text{ave}(v_t^{(i)} \cdot C_i)$;
- **DP global per-sample clipping:** $\bar{V}_t = \text{ave}(v_t^{(i)} \cdot c)$;

where $0 < c', c, C_i \leq 1$ are clipping factors and ‘ave’ is the average. Notice that $c = \min_i C_i$ and hence even though the global clipping is performing a batch clipping, it still requires the $|I_t|$ per-sample clipping factors (which needs to compute the per-sample gradients and their norms) and hence is different from non-DP batch clipping. See Table 5.

	non-DP clipping	DP local clipping	DP global clipping
Need per-sample gradient	No	Yes	Yes
Batch clipping	Yes	No	Yes

Table 5: Comparison of different clippings with respect to whether per-sample gradient information is needed and whether the operation can be applied on the batch as a whole.